Velocity variations associated with the large 2010 eruption of Merapi volcano, Java, retrieved from seismic multiplets and ambient noise cross-correlation

Agus Budi-Santoso, Philippe Lesage

▶ **To cite this version:**

Agus Budi-Santoso, Philippe Lesage. Velocity variations associated with the large 2010 eruption of Merapi volcano, Java, retrieved from seismic multiplets and ambient noise cross-correlation. Geophysical Journal International, 2016, 206 (1), pp.221-240. 10.1093/gji/ggw145 . hal-01416250

HAL Id: hal-01416250
https://hal.science/hal-01416250

Submitted on 14 Dec 2016

HAL is a multi-disciplinary open access archive for the deposit and dissemination of scientific research documents, whether they are published or not. The documents may come from teaching and research institutions in France or abroad, or from public or private research centers.

L'archive ouverte pluridisciplinaire **HAL**, est destinée au dépôt et à la diffusion de documents scientifiques de niveau recherche, publiés ou non, émanant des établissements d'enseignement et de recherche français ou étrangers, des laboratoires publics ou privés.

Geophysical Journal International

Geophys. J. Int. (2016) **206,** 221–240
Advance Access publication 2016 April 13
GJI Mineral physics, rheology, heat flow and volcanology

doi: 10.1093/gji/ggw145

Velocity variations associated with the large 2010 eruption of Merapi volcano, Java, retrieved from seismic multiplets and ambient noise cross-correlation

Agus Budi-Santoso[1,2] and Philippe Lesage[2]

[1]*Badan Geologi, Jalan Diponegoro No.* 57, 40122 *Bandung, Indonesia. E-mail: agus.budi@esdm.go.id*
[2]*ISTerre, CNRS, Université Savoie Mont Blanc, IRD* 219, *F-*73376 *Le Bourget du Lac Cedex, France*

Accepted 2016 April 11. Received 2016 April 9; in original form 2015 August 24

SUMMARY

We present a study of the seismic velocity variations that occurred in the structure before the large 2010 eruption of Merapi volcano. For the first time to our knowledge, the technique of coda wave interferometry is applied to both families of similar events (multiplets) and to correlation functions of seismic noise. About half of the seismic events recorded at the summit stations belong to one of the ten multiplets identified, including 120 similar events that occurred in the last 20 hr preceding the eruption onset. Daily noise cross-correlation functions (NCF) were calculated for the six pairs of short-period stations available. Using the stretching method, we estimate time-series of apparent velocity variation (AVV) for each multiplet and each pair of stations. No significant velocity change is detected until September 2010. From 10 October to the beginning of the eruption on 26 October, a complex pattern of AVV is observed with amplitude of up to ± 1.5 per cent. Velocity decrease is first observed from families of deep events and then from shallow earthquakes. In the same period, AVV with different signs and chronologies are estimated from NCF calculated for various station pairs. The location in the horizontal plane of the velocity perturbations related with the AVV obtained from NCF is estimated by using an approach based on the radiative transfer approximation. Although their spatial resolution is limited, the resulting maps display velocity decrease in the upper part of the edifice in the period 12–25 October. After the eruption onset, the pattern of velocity perturbations is significantly modified with respect to the previous one. We interpret these velocity variations in the framework of a scenario of magmatic intrusion that integrates most observations. The perturbation of the stress field associated with the magma migration can induce both decrease and increase of the seismic velocity of rocks. Thus the detected AVVs can be considered as precursors of volcanic eruptions in andesitic volcanoes, without taking their sign into account.

Key words: Volcano seismology; Magma migration and fragmentation; Volcano monitoring.

1 INTRODUCTION

The forecasting of volcanic eruption is based on the detection of precursory phenomena and on their analysis with the help of physical, statistical or empirical models. The most frequently reported precursors are increases of seismic activity, ground deformations and variations of the flux and composition of gas. In a small number of cases, slight changes in the velocity of seismic waves have been observed prior some eruptions.

In a pioneering study based on seismic multiplets analysis, Ratdomopurbo & Poupinet (1995) detected a velocity increase of up to 1.2 per cent during the 4 months preceding the 1992 eruption of Merapi volcano, Indonesia. Using data of an active source experiment (Wegler & Luhr 2001), Wegler *et al.* (2006) observed an increase of seismic velocity of up to 0.23 per cent in 2 weeks until 3 d after the 1998 eruption of Merapi. At Piton de la Fournaise volcano, Reunion Island, continuous monitoring of the seismic velocity has revealed velocity decreases of the order of 0.05 per cent a few weeks before eruptions (Brenguier *et al*. 2008). Long-term velocity variations, related with episodes of inflation or deflation of the volcanic edifice, were also detected on this volcano (Rivet *et al*. 2014; Sens-Schönfelder *et al*. 2014). A temporary decrease of 0.8 per cent of the seismic velocity was observed starting 2 d before a phreatic eruption of Mt Ruapehu, New Zealand, in 2006 (Mordret *et al*. 2010). A reduction of the phase velocity of Rayleigh waves of up to 1.5 per cent, followed by subsequent recovery, was

© The Authors 2016. Published by Oxford University Press on behalf of The Royal Astronomical Society.

Downloaded from http://gji.oxfordjournals.org/ at Biblio Planets on May 20, 2016

estimated by Nagaoka *et al*. (2010) before the 2008 eruption of Mt Asama. The dike intrusion and caldera formation at Miyakejima volcano, Japan, in 2000 was accompanied by a velocity increase of up to 3.3 per cent on the flanks of the edifice and a velocity decrease of up to 2.3 per cent in regions close to the caldera (Anggono *et al*. 2012). Using families of volcano-tectonic (VT) events, Cannata *et al*. (2012) found velocity decreases during the 2002–2003 Mt Etna eruption. On the other side, velocity variations associated with eruptive activity were tenuous from 1998 to 2013 in Volcán de Colima, Mexico, which probably reflected the open state of the volcano. However, most of the vulcanian explosions appeared to occur when the seismic velocity was low or decreasing (Lesage *et al.* 2014).

In the best documented examples, the velocity variations display complex patterns and both decreases and increases can be observed at different times or simultaneously in different parts of the structure (Anggono *et al*. 2012; Obermann *et al*. 2013). Thus, although these variations are probably related with stress changes in the structure, detailed interpretation in term of physical processes are still required. Furthermore, velocity changes can also be induced by external forcing. For example, some velocity variations in Merapi are related to changes in ground water level between the dry and wet seasons (Sens-Schönfelder & Wegler 2006). Sharp decreases in seismic velocities have been induced by large tectonic earthquakes in various volcanoes (Nishimura *et al*. 2000, 2005; Battaglia *et al*. 2012; Brenguier *et al*. 2014; Lesage *et al*. 2014). It is thus necessary to identify the various sources of velocity variations and, whenever it is possible, to separate them. The location of the velocity perturbations in the structure is very useful for this purpose. An approach based on the assumption that coda waves are multiply scattered surface waves (Pacheco & Snieder 2005) was developed to map the velocity changes in the horizontal plane (Larose *et al*. 2010; Froment 2011; Obermann *et al*. 2013; Planès 2013). It was applied by Obermann *et al*. (2013) to locate the velocity changes associated to eruptions of the Piton de la Fournaise volcano and by Lesage *et al*. (2014) to demonstrate that the velocity decreases induced by tectonic earthquakes are localized in the volcanic edifice, with almost no variations outside of it. Furthermore, Lesage *et al*. (2014), using the frequency dependence of the variations, showed that the sources of perturbation are concentrated at depths less than 800 m below the surface.

When the seismic velocity varies somewhere in the medium, the traveltimes of the waves that propagate through it are slightly modified. This effect is generally more pronounced in the coda waves than in the direct waves because the former are multiple scattered in the structure and their path goes through the perturbed region several times, which induces the traveltime delays to cumulate. These delays can be estimated by comparing the seismograms obtained after the velocity perturbation with a reference record. For this, several techniques are available, either in the time domain (Lobkis & Weaver 2003; Sens-Schönfelder & Wegler 2006; Wegler *et al*. 2006; Rubinstein *et al*. 2007; Anggono *et al*. 2012; Battaglia *et al*. 2012), or in the frequency domain (Poupinet *et al*. 1984; Ratdomopurbo & Poupinet 1995; Nishimura *et al*. 2000, 2005; Brenguier *et al*. 2008; Clarke *et al*. 2011). In both approaches, the two records must be similar enough, which implies that they contain waves that have followed the same path from the source to the receiver. This situation can be fulfilled in three cases: (1) records produced by artificial controlled sources (Nishimura *et al*. 2005; Wegler *et al*. 2006); (2) earthquakes with same focal mechanism and very close sources (seismic multiplets or families of similar events) (Poupinet *et al*. 1984; Ratdomopurbo & Poupinet 1995; Nagaoka *et al*. 2010; Battaglia *et al*. 2012; Cannata 2012) and (3) cross-correlation of ambient seismic noise recorded at two stations (Sens-Schönfelder & Wegler 2006; Brenguier *et al*. 2008; Mordret *et al*. 2010; Anggono *et al*. 2012; Lesage *et al*. 2014). All the previous studies on velocity variation in volcanoes are based on the analysis of only one kind of record.

In this paper, we present a study of the velocity variations that occurred during 1 yr before the large 2010 eruption of Merapi volcano. We use both families of similar events and noise cross-correlation functions (NCF) which allows to investigate the velocity perturbations in various parts of the structure. First, we summarize the volcanic and seismic observations made before and during the eruptive crisis. Then, we describe the procedures used to define the multiplets, to calculate the NCF, and to estimate the variations of traveltime using coda wave interferometry (CWI, Snieder 2006). Finally, we present the velocity perturbations estimated by the two approaches, we carry out the location of the regions where the velocity variations, estimated from NCF, occurred in the structure at various times before the eruption, and we discuss and interpret the results in relation with other observations.

2 ERUPTIVE AND SEISMIC ACTIVITY

Merapi is one of the most active and dangerous volcanoes of Java Island. Common eruptions have typical recurrence of 4–6 yr and are characterized by effusive growth of viscous lava domes which eventually collapse producing pyroclastic flows. Transitions from effusive to explosive regimes also occur with much longer recurrence intervals. They are characterized by large sub-plinian eruptions with volcanic explosivity index (VEI) of 3–4 associated with column collapses and pyroclastic density currents that can travel more than 15 km from the summit. The last explosive eruptions took place in 1872, 1930 and finally in 2010 (Voight *et al*. 2000; Surono *et al*. 2012). The 2010 eruption started on 26 October with an explosive phase. The magmatic phase initiated on 2010 November 1 and reached its paroxysm on 2010 November 4–5, producing pyroclastic density currents that extended 16 km from the summit. The dense rock equivalent volume of erupted juvenile material is $20–50 \times 10^6$ m^3 which corresponds to a VEI of 4. The eruptive crisis was preceded by the unrest of the seismic activity below the volcano. The first related events formed a series of four small seismic swarms 12–4 months before the eruption. Much stronger increase of the seismicity started on the beginning of September, including larger and larger numbers of VT, multiphase (MP) or hybrid, events (Budi-Santoso *et al*. 2013; Budi-Santoso 2014), and some low-frequency (LF), or long-period (LP) and very long-period (VLP) events (Jousset *et al*. 2013). The total cumulative seismic energy release reached three times the maximum energy release before the previous effusive eruptions. The rate of seismicity presented a marked acceleration in the weeks preceding the eruption. This behaviour allowed the use of the material failure forecast method (FFM, Voight 1988), with which consistent and precise estimation of the eruption time was obtained in hindsight within 6 d before the first explosion (Budi-Santoso *et al*. 2013). The hypocenters of the VT events are concentrated in two clusters at [2.5–5] km depth and at less than 1.5 km below the summit. An aseismic zone appears at [1.5–2.5] km depth, a feature that has been present for at least 20 yr (Ratdomopurbo 1995; Ratdomopurbo & Poupinet 2000) and that may correspond to a poorly consolidated layer of altered material (Budi-Santoso *et al*. 2013). VT events that are located in the deep and shallow clusters are called VTA and VTB, respectively.

Downloaded from http://gji.oxfordjournals.org/ at Biblio Planets on May 20, 2016

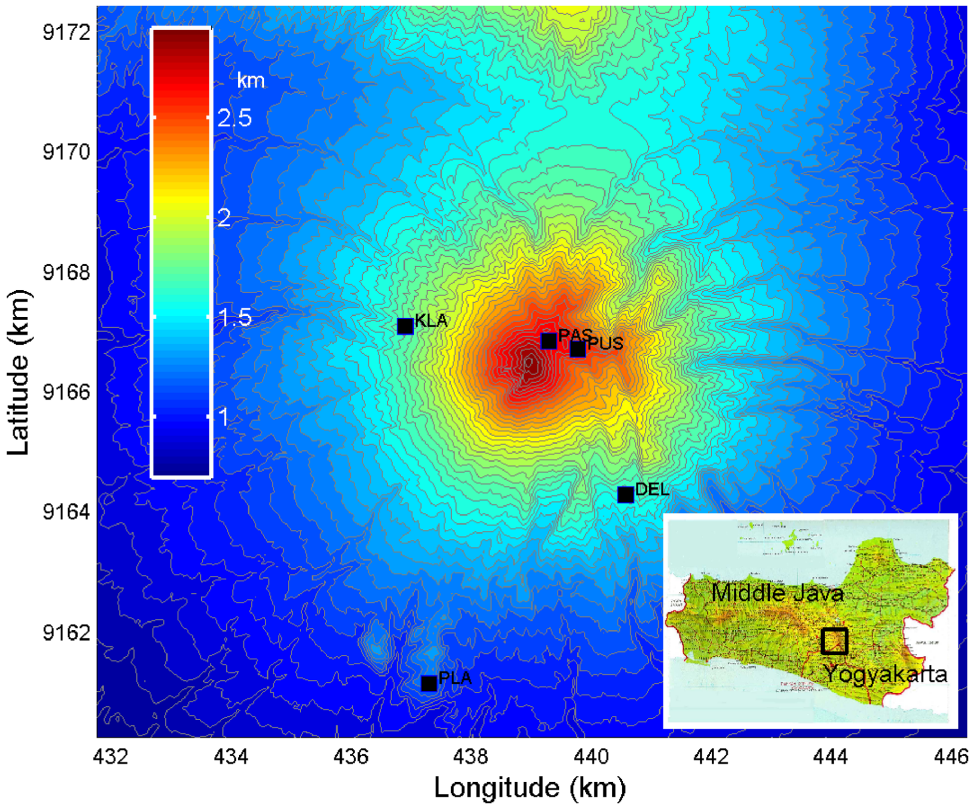

Figure 1. Map of the volcano displaying the position of the permanent short-period seismic stations and the broadband station PAS used in this study. Geographical location is shown in inset.

Ground deformations were monitored by electronic distance measurements (EDM). The first evidence of unrest was observed in November 2009 as a small inflation. From 2010 September 20 to October 26, a line between the crater wall and the southern flank displayed shortening with accelerated rate reaching 50 cm d^{-1} just before the eruption onset. The total shortening was of about 3 m (Surono *et al*. 2012). The displacement rate of this line showed a small decrease on 18–20 October. The other EDM lines did not present significant length variations, which suggests that the observed deformation corresponds to the anelastic outward movement of part of the summit. This block eventually was expulsed by the first explosions. The large volume of erupted material, the strong pre-eruptive deformation and the marked increase of seismicity are all consistent with the intrusion of a large amount of magma through a relatively narrow conduit that resulted in rock damaging and conduit enlargement (Budi-Santoso *et al*. 2013).

3 DATA PROCESSING AND METHODS

3.1 Seismic network

The permanent seismic network consists of four short-period (SP) stations equipped with L4C and L22 seismometers and located at less than 6 km from the crater. Signals are transmitted by radio with VHF modulation and are digitized by a Guralp DM16S acquisition system with 16 bits accuracy and sampling frequency of 100 Hz. All these instruments were replaced by new equipments at the beginning of 2010. In complement, up to six broad-band (BB) stations equipped with CMG-40TD seismometers with period of 60 s were operated since July 2009. Some breakdowns of the digital stations or of the GPS clocks reduced the amount of data available during the pre-eruptive period. However, part of the records obtained during clock failures could be re-synchronized using a procedure based on noise cross-correlation (Stehly *et al*. 2007; Sens-Schönfelder 2008). Only the SP stations (PUS, KLA, DEL and PLA) and the BB station PAS could be used in this research (Fig. 1).

3.2 Seismic multiplets

Families of earthquakes with similar waveforms were identified by calculating correlation coefficients between the pairs of events. Data used here are from the SP station PUS and the BB station PAS recorded from October 2009 to October 2010. PUS and PAS stations are located at 0.7 and 0.5 km from the summit, respectively, and 0.5 km from each other. PAS stopped recording on 23 October, 3 d before the eruption onset. First, an algorithm of automatic event detection, using the LTE/STE ratio (see Appendix A) was applied. The standard deviation of the differences between automatic and manual pickings of arrival times is about 0.015 s with this method. Then the selected records were band-pass filtered (0.5–8 Hz) and cross-correlation coefficients were calculated for each pair of events in 1.7-s-long windows starting 0.5 s before the arrival time. Families were formed using a hierarchical clustering algorithm available in the Matlab Correlation Toolbox (West 2008). Correlation threshold of 0.78 and 0.75 were used for stations PUS and PAS, respectively. The largest value is due to a lower signal-to-noise ratio at the SP station.

Downloaded from http://gji.oxfordjournals.org/ at Biblio Planets on May 20, 2016

3.3 Cross-correlation functions of ambient seismic noise

Daily NCF were calculated for the six pairs of SP stations. Both experimental and theoretical works have demonstrated that the correlation functions of diffuse wavefield, such as seismic ambient noise, are directly related to the Green functions between the recording stations (Weaver & Lobkis 2001; Campillo & Paul 2003). In this study, we processed continuous seismic recordings obtained by the permanent stations for about 1 yr. We applied usual data processing that includes mean and trend removal, band-pass filtering (0.125–2 Hz), spectral whitening and one bit normalization (Bensen *et al*. 2007; Lesage *et al*. 2014). We checked that the one bit normalization does not produce any spurious signal in the correlation functions (see Appendix B). Some corrections for clock synchronization and polarity anomaly were performed when needed. Correlation functions were first calculated on 20 min-long data windows and then stacked over 24 hr.

3.4 Estimation of apparent velocity variations

Velocity variations in the medium induce changes in the traveltime of seismic waves, especially in the coda. The corresponding delays δt can be estimated by CWI using the stretching method (Lobkis & Weaver 2003; Sens-Schönfelder & Wegler 2006; Snieder 2006). In this method, the current record, which can be either an event belonging to a multiplet or a daily NCF, is compared with a reference which can be the stack of all the events of the multiplet or the stack of the NCF obtained during a period of volcanic quiescence. The reference is stretched or compressed in time by a small factor, the stretching coefficient ε. The correlation coefficients between the current record and the stretched reference are calculated as a function of ε. The value ε_{M} of the stretching coefficient that gives the best correlation is equal to the relative delay: $\varepsilon_M = \frac{\delta t}{t}$, where t is the mean time lag of the delay window used. If the relative velocity variation is homogeneous in the medium, it is equal to $-\varepsilon_{\mathrm{M}}$. However, it most cases, this assumption is not valid and $-\varepsilon_{\mathrm{M}}$ must be considered as an 'apparent velocity variation' (AVV). The AVV can be estimated in various overlapping delay windows in the coda of the events or of the correlation functions. It is thus a function of the time lag t. When the correlation coefficient between the daily and the reference NCF is smaller than 0.6, the AVV is not significant and the corresponding stretching coefficient is discarded for the subsequent calculations. Errors in the stretching coefficient are calculated using the relation derived by Weaver *et al*. (2009). They depend on the correlation coefficient between the records, the frequency band, the signal frequency and the delay window used. In the case of multiplets, a unique delay window of 6 s starting 1 s after the arrival time was used. For the NCF, the time lag of the delay window depends on the station pair considered and is generally in the range [10–30] s. Then, the correlation functions in the interval of ± 2 d around the current date were stacked in order to obtain more reliable NCF and smoother velocity variations.

3.5 Location of velocity perturbations in the horizontal plane

The location of velocity perturbation within the structure can be estimated by using an approach based on the propagation of diffuse wavefields (Larose *et al*. 2010; Froment 2011; Obermann *et al*. 2013; Planès 2013). The coda is mainly composed of multiple scattered surface waves that propagate following a random walk process in a 2-D medium (Pacheco & Snieder 2005). A distribution of velocity perturbations dv/v($\boldsymbol{x}_0$) produces traveltime variations as:

$$\delta t(t) = -\int_s K(s_1, s_2, x_0, t)\frac{\delta v}{v}(x_0)\mathrm{d}S(x_0), \tag{1}$$

where s_1 and s_2 are the positions of the source and station (or both stations in the case of NCF), x_0 is the location of the perturbations, and K is a sensitivity kernel given by:

$$K(s_1, s_2, x_0, t) = \frac{\int_0^t p(s_1, x_0, t') \,.\, p(x_0, s_2, t - t')\mathrm{d}t'}{p(s_1, s_2, t)}, \tag{2}$$

where p represents the intensity of the wavefield between two points as a function of time (Pacheco & Snieder 2005). Here we used a solution of the radiative transfer equation in 2-D (Shang & Gao 1988; Sato 1993; Paasschens 1997; Obermann *et al*. 2013; Planès 2013), as:

$$p(r,t) = \frac{\mathrm{e}^{-vt/l}}{2\pi r}\delta(vt - r) + \frac{\Theta(vt-r)}{2\pi l vt}\left(1-\frac{r^2}{v^2t^2}\right)^{-\frac{1}{2}} \exp\left[l^{-1}(\sqrt{v^2t^2-r^2}-vt)\right], \tag{3}$$

where v is the wave velocity, r is the distance between source and receiver, l is the transport mean free path and Θ is the Heavyside function. Fig. 2 displays sensitivity kernels calculated for two time lags. Traveltime variations are related to the estimated AVVs:

$$\frac{\delta t(t)}{t} = \varepsilon_M(t) = -\left.\frac{\delta v(t)}{v}\right|_{app}. \tag{4}$$

The distribution $\delta v/v(\mathbf{x_0})$ can be estimated by solving eq. (1) as a linear inverse problem (Tarantola & Valette 1982; Froment 2011; Obermann *et al*. 2013; Lesage *et al*. 2014) which can be written in a matricial form as:

$$d = Gm. \tag{5}$$

d is the vector of data, that is the AVV estimated for different pairs of stations and various time delays (Fig. 3), G is a matrix which contains the sensitivity kernels K and m is the model vector $\delta v/v(x_0)$. A covariance matrix of the model is introduced in order to produce smooth models (Lesage *et al*. 2014). It is characterized by a correlation length λ and an *a priori* standard deviation σ_{m} that are selected using the L-curve criterion (Hansen 1992). Following this criterion, the optimal parameters are $\lambda = 1$ km and $\sigma_{\mathrm{m}} = 0.1$. We focused the location on an area of 15×15 km^2 centered on the volcano with grid spacing of 0.3 km and we took $v = 1.3$ km s^{-1} as surface wave velocity. For the transport mean free path l, we used the value of 100 m estimated by Wegler & Luhr (2001) from an active source experiment on Merapi. Some tests with various values of l and v showed that the location of velocity perturbations is only weakly dependent of these parameters. We generally used the AVV estimated for five time delays per station pair in the range [5–35] s (Fig. 3), yielding a total of 30 components for the data vector d.

Downloaded from http://gji.oxfordjournals.org/ at Biblio Planets on May 20, 2016

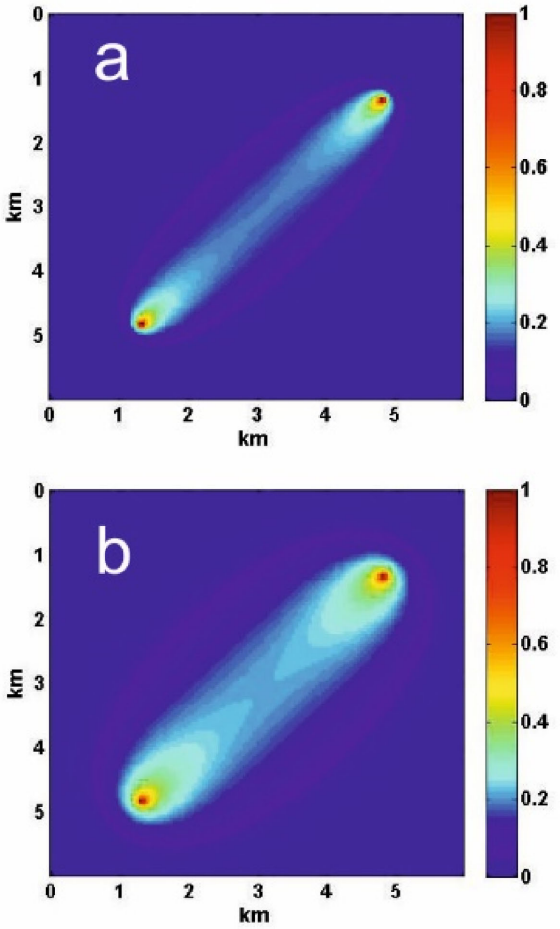

Figure 2. Examples of sensitivity kernels (eq. 2) based on the radiative transfer approximation in 2-D. Distance between receivers is 5 km, mean free path is $l = 100$ m, wave velocity is $v = 1.3\,\mathrm{km\,s^{-1}}$, time lags are 10 s (a) and 30 s (b).

4 RESULTS

4.1 Seismic multiplets

Nine families of similar events, named also multiplets or clusters, were obtained at both stations PUS and PAS. A tenth family was formed by about 120 events that occurred in the 20 hr preceding the first explosion. They were recorded only by PUS because station PAS was no longer available at that moment. A total of 209 events among 393 detected events at PAS (53 per cent) and 322 among 795 at PUS (41 per cent) belong to the multiplets (Fig. 4). A few events of multiplets 2, 3 and 6 are part of the seismic swarms that occurred in December 2009 and June 2010. They are not shown in Fig. 4. Clusters 1 and 2 include LF events whose dominant frequencies are below 3 Hz. The remaining clusters consist of VT events characterized by dominant frequencies between 3 and 6 Hz.

Relative location of the events belonging to the clusters has been carried out using program HYPODD (Waldhauser & Ellsworth 2000) based on the method of double difference. Average uncertainties of 50 and 120 m were obtained for the horizontal and vertical relative positions, respectively. Although these values are formal errors and are smaller than the real uncertainties, the precision of this approach appears to be better than that of the absolute location done by Budi-Santoso *et al*. (2013). The results of the relative locations are consistent, but less spread, with those of the absolute hypocentre determinations (Fig. 5). The sources are distributed in a narrow cylinder below the crater at two depth ranges. Deep VTA events that belong to clusters 4, 5 and 9 are located between 2.3 and 3 km beneath the summit, while shallow LF and VTB earthquakes forming the other clusters occurred at less than 1.5 km deep. The histogram of depth distribution shows that the largest population is located at [0.5–1] km below the summit (Fig. 5). It is actually mainly composed by cluster 10 that occurred during the day preceding the eruption. The aseismic zone appears clearly in the depth distribution between 1.5 and 2.3 km. Fig. 6 displays the source elevations as a function of time, together with histograms of the numbers of VTA and VTB events. The deep VTA events occurred during the first part of the pre-eruptive period in September and until mid-October. After that, while VTA activity was diminishing, a sharp increase of the rate of VTB events took place during the week before the eruption of 26 October.

4.2 AVVs estimated with multiplets

Figs 7 and 8 display the AVVs estimated using the multiplet events. Separate plots were done per station and for the deep and shallow clusters (Figs 7a and b), as well as for cluster 10 (Fig. 8). Note that the corresponding errors, calculated with the Weaver's formula (Weaver *et al*. 2009) are of the order of 0.04 per cent. In general, the results obtained with records from the broad-band station PAS are more consistent than those from PUS. Some events belonging to clusters 2, 3 and 6 occurred as early as on October 2009 and June 2010. The AVV estimated with these events indicate that no significant velocity variations took place in the volcano until September 2010. For most of the deep clusters, slight decreases of velocity took place in September and early October 2010, followed by sharp decreases of a few tenths of per cent around 10 October. In the case of shallow multiplets, after a small increase detected with cluster 2 at PAS in the first days of September 2010, the velocity remained relatively constant, although a slight decrease can be observed for clusters 1 and 6. In the period from 2010 October 13 to 17, rapid velocity decreases of 0.5–1.5 per cent occurred for all the shallow clusters. For some of them, the decreasing trend continued until the first explosion, while for other multiplets, the apparent velocity turned to increase just before the eruption onset. The analysis of the events of cluster 10 provides a good temporal resolution for the AVV (Fig. 8). During the 20 hours that preceded the first explosion, the estimated velocity presented fluctuations of about ± 0.3 per cent. Interestingly, in several instances, the minimum values of the velocity coincided with the occurrence of large VTB events that produced the saturation of the records. The largest VT event of the pre-eruptive sequence occurred on 2010 October 25 at 20:00 UTC at shallow depth and coincides with a sharp velocity decrease.

4.3 AVVs estimated from noise cross-correlation functions

Stacked cross-correlation functions of ambient noise (NCF), calculated for all the station pairs, are presented in Fig. 9. The NCF are not symmetrical because the sources of noise are dominantly located in the ocean at the South of the volcano (Budi-Santoso 2014). The most energetic sides of the NCF, with time delays in the range [10–30] s, were used for the calculations of AVV. Examples of daily NCF for pair DEL-PLA and the period from June to October 2010 are displayed in Fig. 10. As for the other pairs, their waveforms show good temporal stability, which is a required condition for applying the stretching method. The AVV calculated from NCF

Downloaded from http://gji.oxfordjournals.org/ at Biblio Planets on May 20, 2016

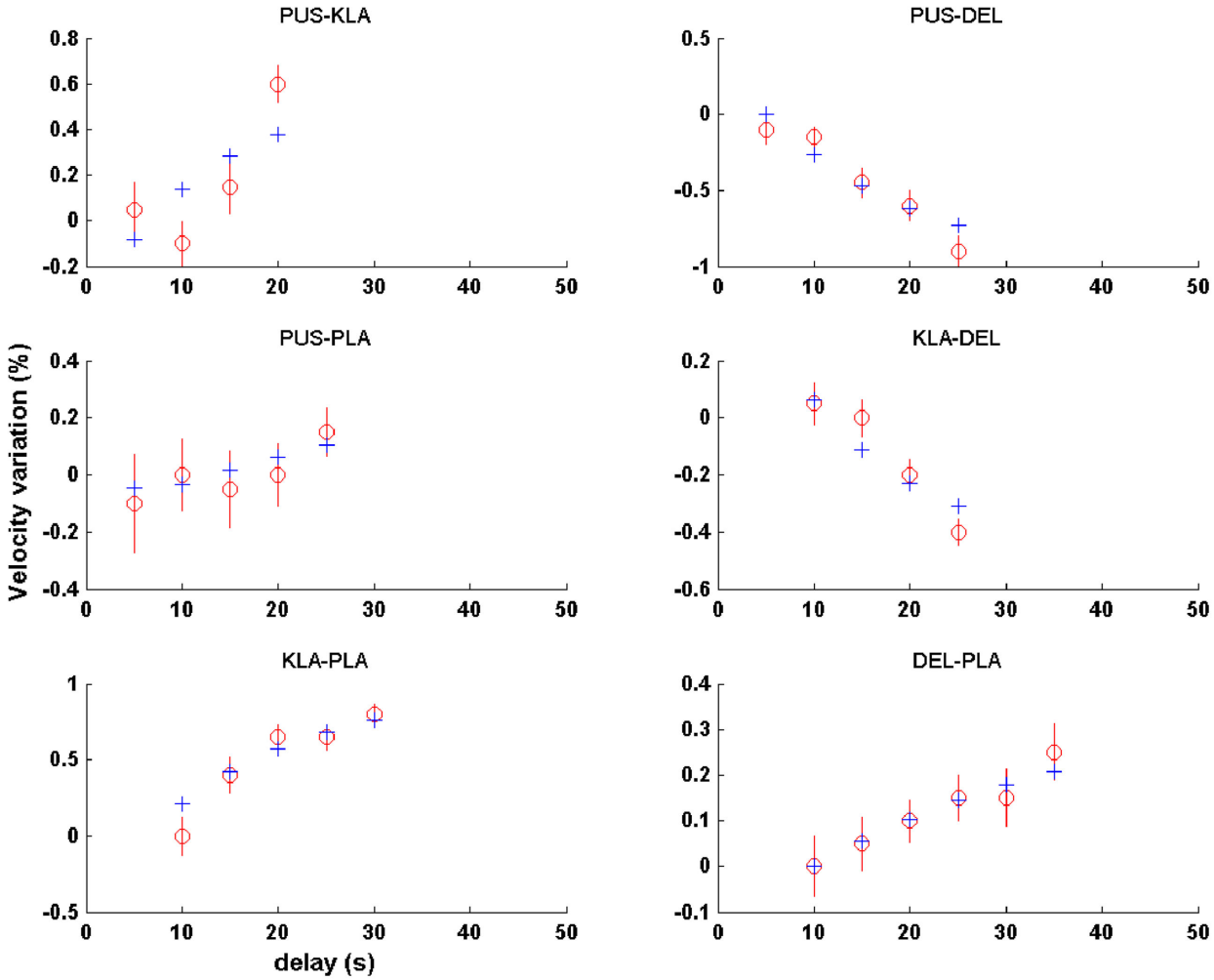

Figure 3. Apparent velocity variations estimated from NCF for various time delays (red circles with error bars) and calculated from the model of perturbation location (blue crosses) for the six station pairs. The period used to calculate the AVV here is 12–21 October.

appeared to be partly correlated with the rainfall, with long term velocity decreases observed during the rainy season. We followed Sens-Schönfelder & Wegler (2006) who obtained similar observations at Merapi and showed that velocity variations can be described by a hydrological model of ground water level (GWL) based on the Darcy's law. We adjusted the model parameters in order to obtain a good fit between the GWL model and the observed AVV (Budi Santoso 2014). Then we calculated corrected velocity variations by subtracting the GWL model from the AVV (Fig. 11). It was not possible to apply the same procedure and to correct AVV estimated from multiplets because the time-series of similar events are not continuous. However, the rain corrections estimated for AVV from NCF are small during the period of occurrence of the multiplets. Thus the effects of water table level are probably also small on AVV from multiplets. The AVV, corrected for rainfall effect, obtained for the six station pairs in the period from 2010 August 1 to the eruption are displayed in Fig. 12. For this calculation, the reference NCF is the stack of the daily NCF from 2010 August 15 to 2010 September 10. From September 2009 to beginning 2010, the NCF do not display good stability and the corresponding AVV are not very reliable. This is mainly due to the instrumental problems encountered before the hardware replacement. However, it seems that no velocity variations occurred in that period.

4.4 Chronology of velocity variations

Before 2010 October 12, the AVV obtained from NCF present slight variations, with possibly a small decrease trend (Fig. 12). After this date, the velocity variations are larger with amplitudes of up to 1 or 1.5 per cent. However, their signs and chronologies are not all consistent. Indeed, increasing AVV at some pairs (KLA-PLA, DEL-PLA and PUS-KLA) occurred simultaneously with decreases at pair PUS-DEL, while almost no changes were detected for pairs KLA-DEL and PUS-PLA. These trends eventually changed at different moment according to the station pair. For example, the velocity turned to decrease on 2010 October 23 for pair PUS-KLA while it started increasing on 2010 October 20 for PUS-DEL.

Fig. 12 shows also the velocity variations estimated from a selected set of representative multiplets, together with histograms of seismic activity from August to November 2010. Taking into account the behaviour of the seismicity and of the AVV, six phases can be distinguished. A first phase corresponds to the quiescent period before the seismic unrest that began in early September 2010. No significant velocity variations are detected during this phase. The second phase ended on 2010 October 12 and corresponds to relatively stable velocities although small variations are obtained for clusters 2 and 4. At the end of this phase, a small sharp velocity

Downloaded from http://gji.oxfordjournals.org/ at Biblio Planets on May 20, 2016

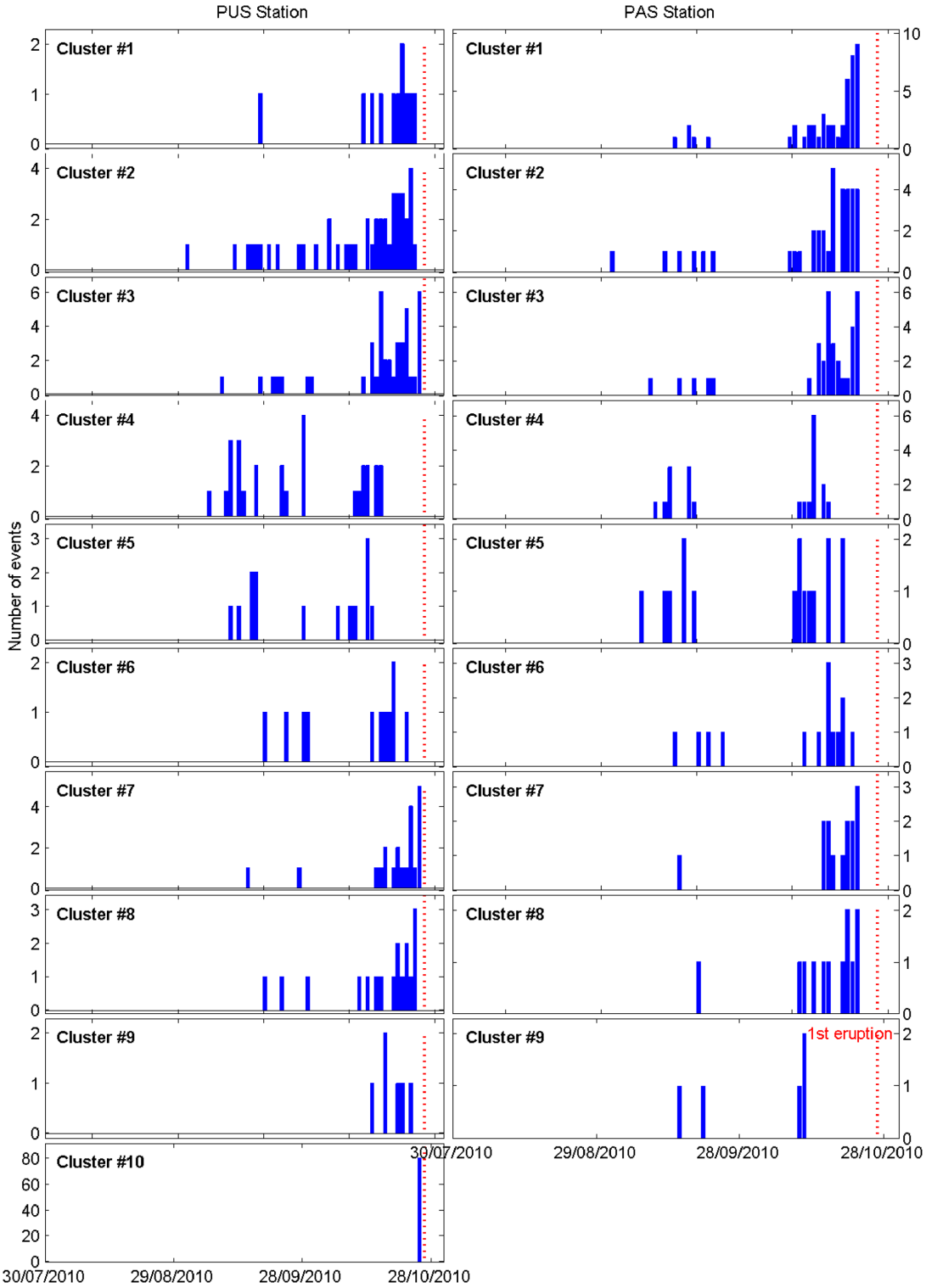

Figure 4. Histograms of the daily occurrence of similar events recorded at PUS (left-hand panels) and PAS (right-hand panels) stations.

decrease is detected for the deep multiplet 4. The third phase (2010 October 12–21) is associated with velocity decreases for shallow clusters 2 and 3 and pair PUS-DEL, together with velocity increase for DEL-PLA and KLA-PLA. The end of this phase is related to the change of trend from decrease to increase for cluster 3 and pair PUS-DEL that occurred on 2010 October 21. Phase four (2010 October 21–25) corresponds to increases of velocity at almost all the station pairs. It is also associated with the marked increase of the rate of VTB events while the VTA activity was declining. Large LF events occurred during this period. The fifth phase took place during the last day before the first explosion of 2010 October 26. It is associated with a velocity decrease for the last two events of cluster 2 and for pairs PUS-KLA, PUS-PLA and, at a smaller extent, KLA-DEL. The events of cluster 10 occurred during this phase.

Downloaded from http://gji.oxfordjournals.org/ at Biblio Planets on May 20, 2016

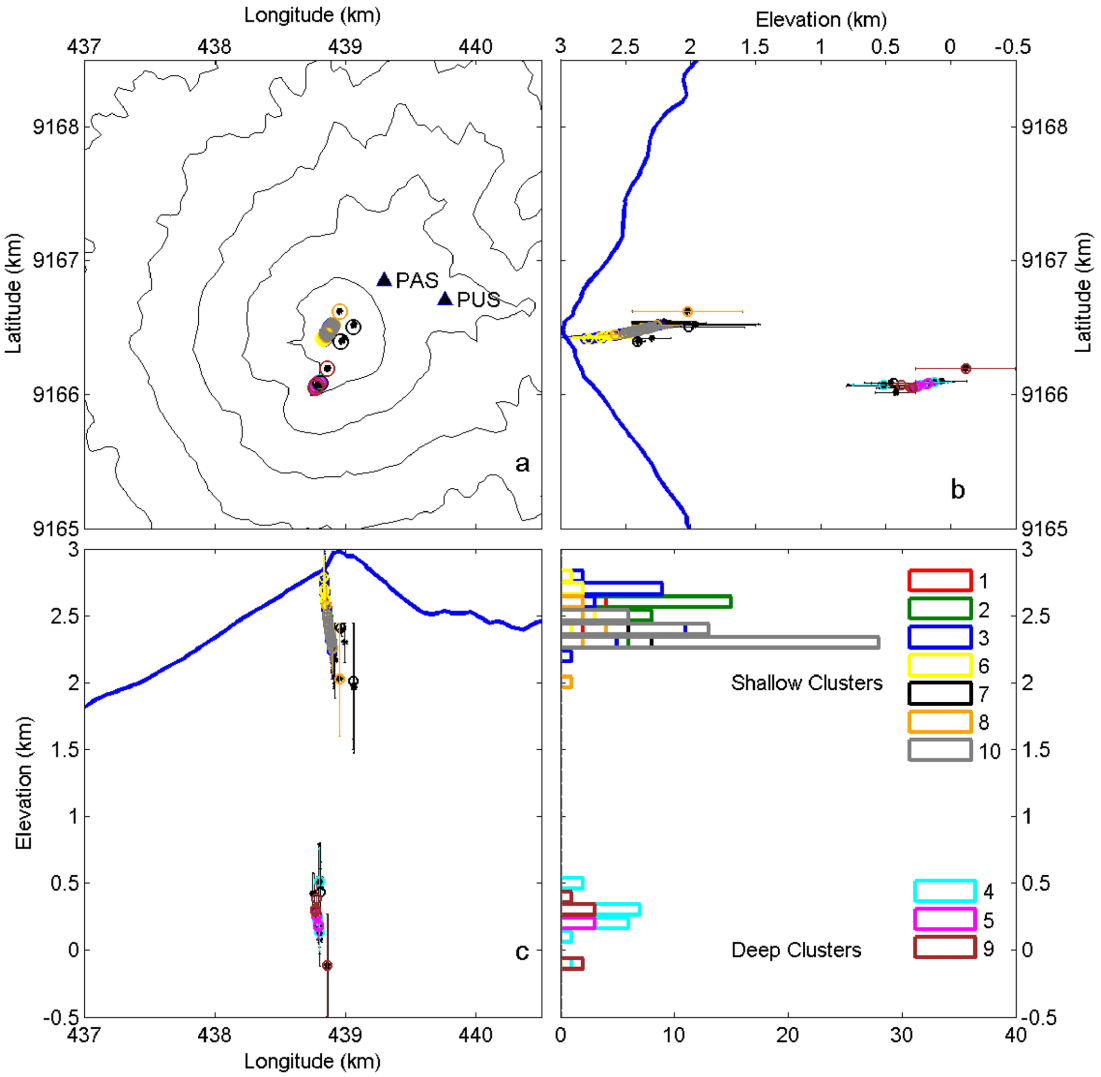

Figure 5. Relative location of the events that belong to the multiplets. HypoDD program was used with an homogeneous velocity model with $Vp = 3$ km s^{-1} and $Vp/Vs = 1.86$. (a) Map, (b) N–S cross-section, (c) E–W cross-section. (d) Histogram of depths. The errors on vertical location, plotted in panels (b) and (c), are smaller than 0.5 km. The colours of hypocentres, displayed in inset of panel (d), indicate the clusters events belong to.

A sixth phase can be defined during the explosive activity from 2010 October 26 to 2010 November 3, which preceded the paroxysmal phase of the eruption and the destruction of the stations. During this period, velocity decreases are observed at almost all the pairs. At the end of this phase, on 2 and 3 November, a velocity increase is detected again at pairs PUS-DEL, KLA-DEL and KLA-PLA.

4.5 Location of velocity perturbations

We applied the method described above (Section 3.5) to locate the sources of velocity variations estimated from NCF. We used the AVV calculated over three overlapping periods, all starting at the beginning of phase 3 and finishing at the end of phases 3, 4 and 6, respectively (Figs 13a–c). In other words, we consider the velocity variations between a reference state (on 2010 October 12) and three states of the system on 2010 October 21, October 25 and November 3, respectively. When inverting the AVV calculated over shorter intervals, the results are less stable and reliable. During phase 3 (2010 October 12–21), the velocity decreased in the upper part of the edifice, especially on the South flank and a zone of velocity increase appeared at about 4 km South and Southwest from the crater (Fig. 13a). During the interval 2010 October 12–25, the velocity decrease close to the summit and on the South flank was slightly more marked than before, while the zone of velocity increase extended to a ring on the lower flanks at the south, east and north parts of the edifice (Fig. 13b). During the period ending on 2010 November 3, the pattern of velocity changes was significantly modified with respect to the previous periods. Regions of velocity increase are located at the east, west and southwest from the summit, while zones of decreases are concentrated on the southern flank and, at a smaller extent, at the northern side of the structure (Fig. 13c). To validate the estimated distributions of perturbation, the restitution index was calculated from the resolution matrix (Vergely *et al*. 2010; Obermann *et al*. 2013). Values smaller than ∼0.8 indicate that the velocity variation is badly recovered in the corresponding cell. In most part of the structure where significant perturbations appear, the restitution index is close to one (Fig. 13d). However, some regions, on the southern part of the volcano for periods ending on 2010 October 21 and 25 and on the eastern part for the period finishing

Downloaded from http://gji.oxfordjournals.org/ at Biblio Planets on May 20, 2016

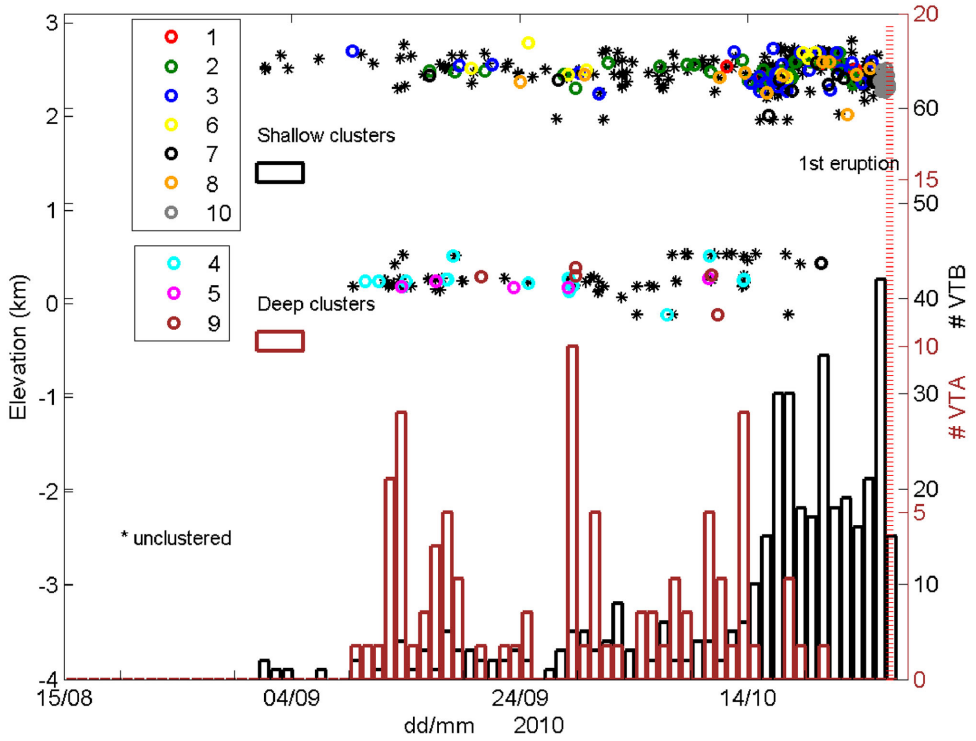

Figure 6. Elevations of events that belong to the multiplets plotted as a function of time for the period of September–October 2010. Clusters are indicated by different colours as shown in the legend. Histograms of the daily numbers of deep VTA and shallow VTB events are shown by brown and black bars, respectively.

on 2010 November 3, are poorly constrained and the corresponding velocity perturbations must be considered as poorly reliable. In all cases, the AVV calculated with the estimated models of perturbation fit well the data, that is the observed AVV for most time delays used (Fig. 3).

5 INTERPRETATION AND DISCUSSION

5.1 Summary of results

A large proportion of earthquakes that occurred before the 2010 eruption belongs to families of similar events. The relative location of their sources confirms that they are distributed into two seismogenic zones below Merapi's crater separated by an aseismic layer about 1 km thick. These sources, which are initially clustered below this layer, migrate upward at mid-October and are concentrated in the shallowest part of the structure in the last days before the eruption. Using the method of CWI, time-series of AVV were estimated from the seismograms of these multiplets. They all display clear velocity decrease of up to 1.5 per cent that began in the period from 2010 October 10 to 17. Velocity variations of the same order of magnitude were obtained by analyzing the coda of seismic noise correlation functions for the six pairs of stations. These variations appeared after 2010 October 10, with different chronologies and signs according to the pair used. The AVV calculated from NCF as a function of time lag in the coda were inverted to estimate the distribution of the velocity perturbations in the structure. Before interpreting these results, it is important to assess their uncertainties and significance.

5.2 Uncertainties

The calculated AVV result from the superposition of several effects which are not all related with volcanic activity. For instance, variations of the distribution of noise sources may modify the NCF and generate spurious AVV (Froment *et al*. 2010). In the case of multiplets, part of the delay variations in the coda can be due to the separation of the sources (Got & Coutant 1997). The rain, through modification of the water table level, induces changes of the seismic velocity in the shallow layers. The corrections for this effect, based on a simple linear model, are probably only partial and some influence of the meteorological phenomena may remain in the corrected time-series. We assume that the AVV calculated during periods of volcanic quiescence are mainly due to the spurious effects and do not reflect modification of the volcano state. The corresponding amplitudes are of a few tenths of per cent. By comparison, the errors on the stretching coefficients calculated by using the relation proposed by Weaver *et al*. (2009) are small. Moreover, the estimation of AVV also depends, to some extent, on the parameters used for the calculations (frequency range, lag interval, smoothing length, etc.). Finally, by taking into account the various effects that can modify or contaminate the observations, we estimate that the uncertainties on the velocity variations associated with the volcanic unrest are of the order of 0.5 per cent. This value is close to the estimation of the effect of non-even distribution of noise sources (Froment *et al*. 2010). Thus, the amplitudes of AVV observed during the pre-eruptive period are only two or three times the corresponding uncertainties. However, the fact that the AVV estimated from multiplets occurred almost simultaneously and those obtained from NCF occurred in a short time interval before the eruption strongly suggests that these variations are mainly related with volcanic phenomena.

Downloaded from http://gji.oxfordjournals.org/ at Biblio Planets on May 20, 2016

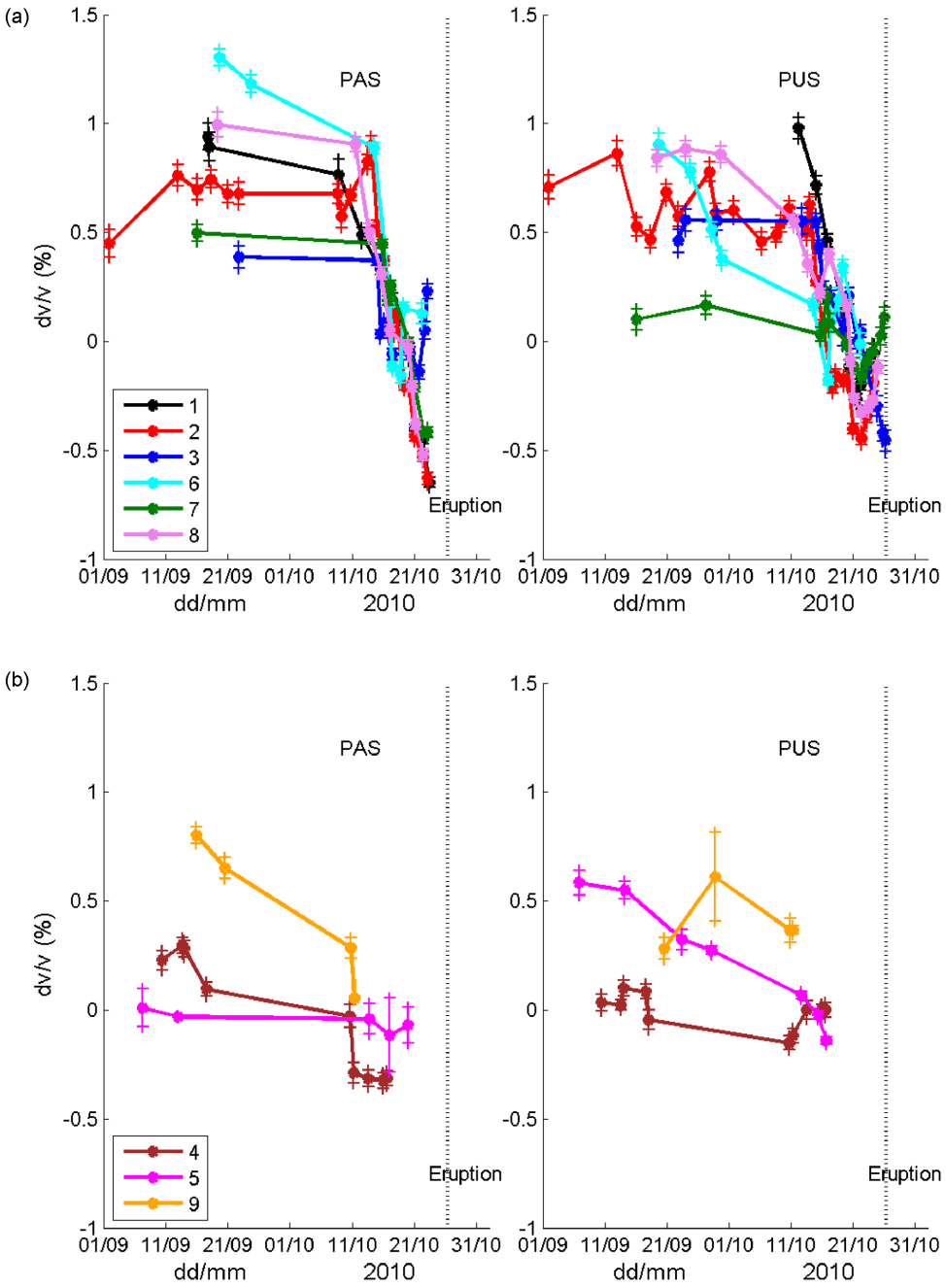

Figure 7. Apparent velocity variations calculated with events of shallow (a) and deep (b) multiplets recorded at PAS (left-hand panels) and PUS (right-hand panels) stations. Vertical dashed line indicates first eruption.

5.3 Significance of AVV

The methods of CWI allow to measure with good sensitivity variations of the traveltime of seismic phases. The relative time variations $\delta t/t$ are related with relative velocity variations $\delta v/v$ in the structure. When these variations are homogeneous in the volume sampled by the waves, $\delta v/v$ is equal to $-\delta t/t$. Otherwise they must be considered as AVVs which are weighted averages of the distribution of the real velocity variations in the structure. When using noise correlation functions (NCF), it can be assumed that their coda are primarily composed of surface waves. In the frequency range used in this study, they are probably sensitive to velocity changes in layers extending from the surface to 3000–5000 m deep. The relationship between traveltime variations and velocity changes (eq. 1) is based on sensitivity kernels (eq. 2) that have saddle-like shapes. Their values are non-null in ellipsoidal regions whose focus are the stations and whose extension increases with increasing time lag in the coda (Fig. 2). These kernels are larger along the line between the stations and are maximal close to them. When using multiplets, the theoretical kernels are defined in three spatial dimensions and their focus are the source and the recording station. Thus, depending on the source depth and position, AVV for multiplets can be sensitive to velocity variations in different parts of the structure. In particular, if a source of multiplet is located close to the conduit, the corresponding AVV can be very sensitive to perturbations due to the intrusion. On the other hand, in a volcanic structure,

Downloaded from http://gji.oxfordjournals.org/ at Biblio Planets on May 20, 2016

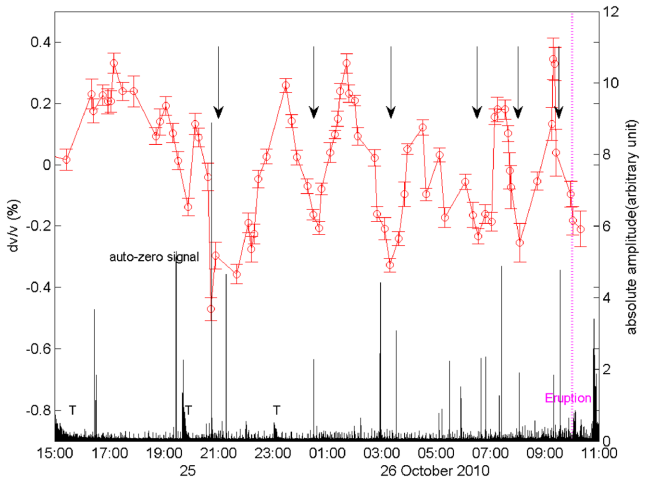

Figure 8. Apparent velocity variations for cluster 10 recorded at PUS station (red line) and maximal amplitude of the seismic events (black vertical line). Occurrence of main VT events are indicated by arrows. Vertical dotted line shows eruption onset.

the heterogeneities that produce multiple scattering of waves forming the coda are probably not randomly distributed. For example, Got & Coutant (1997) showed, using seismic multiplets with sources at 8 km depth, that multiple scattering near the surface dominates the coda at Kilauea volcano. In this example, the sensitivity kernels should be larger close to the surface than at depth. In the case of NCF, the theoretical kernels were used in the inverse problem of locating the velocity perturbations in the structure. As these kernels are based on the propagation of diffuse wavefields, they produce a smoothing effect in the inversion. Consequently, even if the real velocity perturbations are actually well localized in a small region, the pattern obtained in the location process may be much spreader. On the other side, the uncertainties on the observed AVV produce uncertainties on the location of the perturbations. Moreover, with the small number of stations available, the resulting location is not strongly constrained. Taking the uncertainties and lack of constrain into account, we consider that only the main features of the location maps are significant, namely the velocity decrease in the upper part of the edifice before the eruption and the strong modification of the perturbation after the eruption onset.

5.4 Physical origin of velocity variations

Many laboratory experiments have demonstrated that the physical parameters of rocks are stress dependent (Birch 1960; Nur 1971; Lockner *et al*. 1977; Mavko *et al*. 1995; Shapiro 2003). Actually, they mainly depend on the effective pressure P_{eff} which is the difference between the confining pressure P_c and the pore pressure P_p : $P_{\text{eff}} = P_c - P_p$ (Zimmerman *et al*. 1986). When the effective pressure applied on a rock sample is raised, the cracks close yielding the elastic modulus and the seismic velocities to increase (Nur 1971). This effect is enhanced in porous rocks due to the closing of compliant porosity with increasing effective pressure (Eberhart-Phillips *et al*. 1989; Shapiro 2003; Heap *et al*. 2014a). In particular, the variations of velocities, porosity and permeability with pressure can be quite strong in volcanic rocks, as they contain many vesicles and are pervasively microcracked (i.e. Rocchi *et al*. 2004; Stanchits *et al*. 2006). For example Heap *et al*. (2014b) studied the behavior of andesitic rocks from Volcan de Colima, Mexico. They showed that for stress varying from 0 to 32 MPa, *P*- and *S*-waves velocities increase from 2 to 4.2 km s^{-1} and from 1.2 to 2.5 km s^{-1}, respectively. The andesites of Merapi are very similar to those of Volcan de Colima (Heap, personal communication). Therefore, these results probably stand for both volcanoes. Under uniaxial stress, cracks normal to the stress axis are closed while cracks parallel to it are almost unaffected (Nur 1971). At high deviatoric stress level, cracks appear and grow predominantly in the direction parallel to the principal stress axis. During this stage of damaging, the seismic velocities strongly decrease.

On the other hand, due to free surface effect, topography and heterogeneity of volcanoes, a pressure increase in the plumbing system can produce both tensional stresses in some parts and compression in other parts of the structure (Got *et al*. 2013). Therefore,

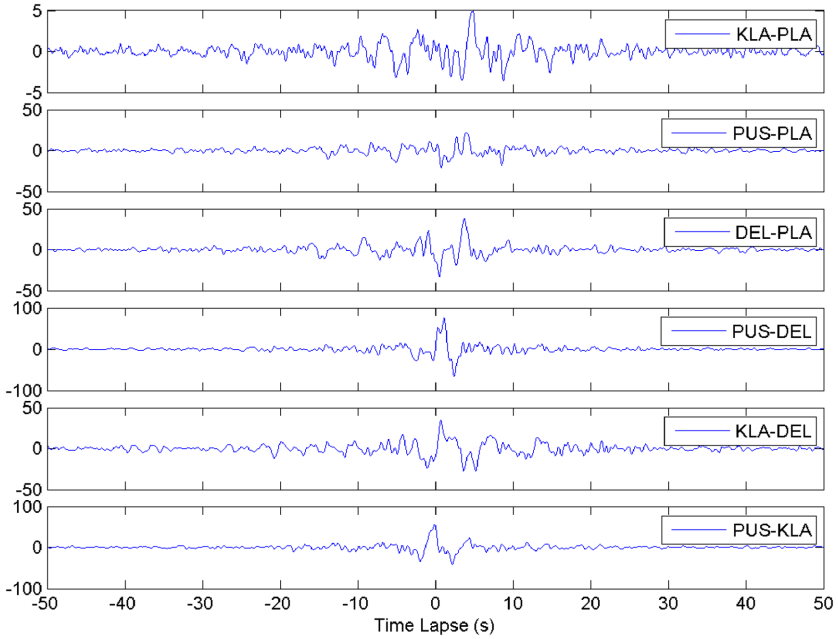

Figure 9. Stacked cross-correlation functions of seismic noise obtained for all the station pairs.

Downloaded from http://gji.oxfordjournals.org/ at Biblio Planets on May 20, 2016

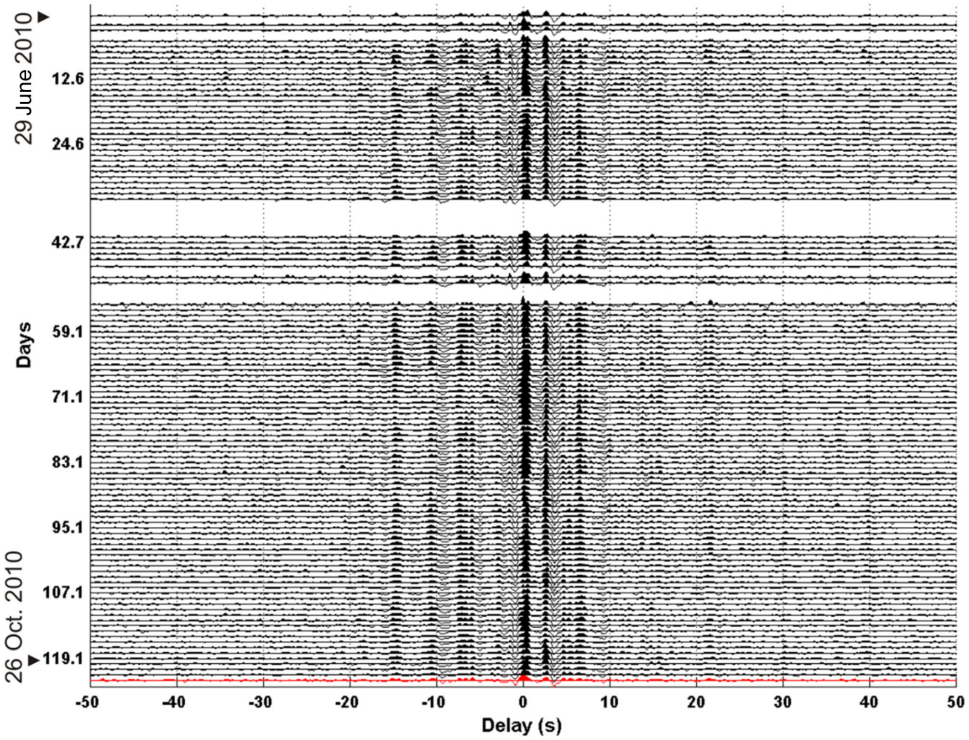

Figure 10. Daily noise cross-correlation functions obtained for pair DEL-PLA from June to October 2010. The frequency range used is [0.125–2] Hz.

taking into account this complexity of the stress fields, the facts that velocity can either increase or decrease with increasing deviatoric stress, and that seismic wave propagation and scattering in volcanic structures are complicate and poorly known phenomena, it appears difficult to propose precise interpretation and modelling of observed AVVs. In other words, the pressure rise in magmatic conduit related to an intrusion can induce both increase and decrease of the velocity depending on time, depth and location of the considered part of the structure with respect to the conduit. The resulting AVV can be thus either positive or negative, according to the relative position of the station pair, or the hypocentre and station when using multiplets, and of the velocity perturbations. As a consequence, only the absolute value of the AVV could be used as precursors of volcanic eruptions without taking the sign of the variation into account. This physical framework is consistent with the velocity variations observed during the pre-eruptive period of Merapi volcano in 2010. It can explain the complex pattern of velocity changes, where velocity increases and decreases are obtained simultaneously at different stations pairs and where delays in the onset of velocity decrease appeared between deep and shallow multiplets.

5.5 Comparison with previous studies

The results obtained in the present work and based on long time-series provide new insights on some previous studies. Using CWI on shallow seismic multiplets, Ratdomopurbo & Poupinet (1995) detected a continuous increase in seismic velocity of the order of 1.2 per cent from April and September 1991, several months before the February 1992 eruption of Merapi volcano. No equivalent velocity variations were obtained months before the 2010 eruption although the later event was much larger than the 1992 eruption. This suggests that part of the increase in 1991 could be associated with the beginning of the dry season and the consecutive falling of the ground water table. Indeed, Sens-Schönfelder & Wegler (2006), using data from a small-aperture array, observed seasonal velocity variations of the order of 1 per cent and interpreted them as the effect of changes in the ground water level. These variations have much larger amplitudes than the seasonal changes observed in the present studies (0–0.3 per cent). This may be due to the behaviour of the area around the array used by these authors and to the fact that the corresponding coda waves sampled shallower layers than in our case. Wegler *et al.* (2006) analysed similar waveforms produced by a repeatable controlled seismic source. They observed, a few days before the 1998 eruption, a velocity increase of the order of 0.1 per cent at one site and a decrease followed by an increase at other site. The small amplitude of the variations may be explained by the relatively large distance of the sources and receivers from the crater and by the very shallow layers sampled by the waves generated by the airgun used as source. However, the sparseness of the obtained values of AVV in this experiment precludes any reliable interpretation.

5.6 Interpretative framework

The monitoring network of Merapi has provided valuable information on the volcanic processes that took place during the pre-eruptive period. This includes the type of seismic events and location of their sources, the level of seismicity and energy release, velocity variations and deformations in the structure. All these observations are consistent with the intrusion of a large batch of magma during the weeks preceding the eruption (Budi Santoso *et al.* 2013). Although the structure of Merapi is poorly known (Koulakov *et al.* 2007; Zulfakriza *et al.* 2014), an aseismic zone has been identified between 1.5 and 2.5 km below the crater. This layer seems to be a permanent feature as it has been observed since at least 1992 (Ratdomopurbo & Poupinet 2000; Wassermann & Ohrnberger 2001; Hidayati *et al.*

Downloaded from http://gji.oxfordjournals.org/ at Biblio Planets on May 20, 2016

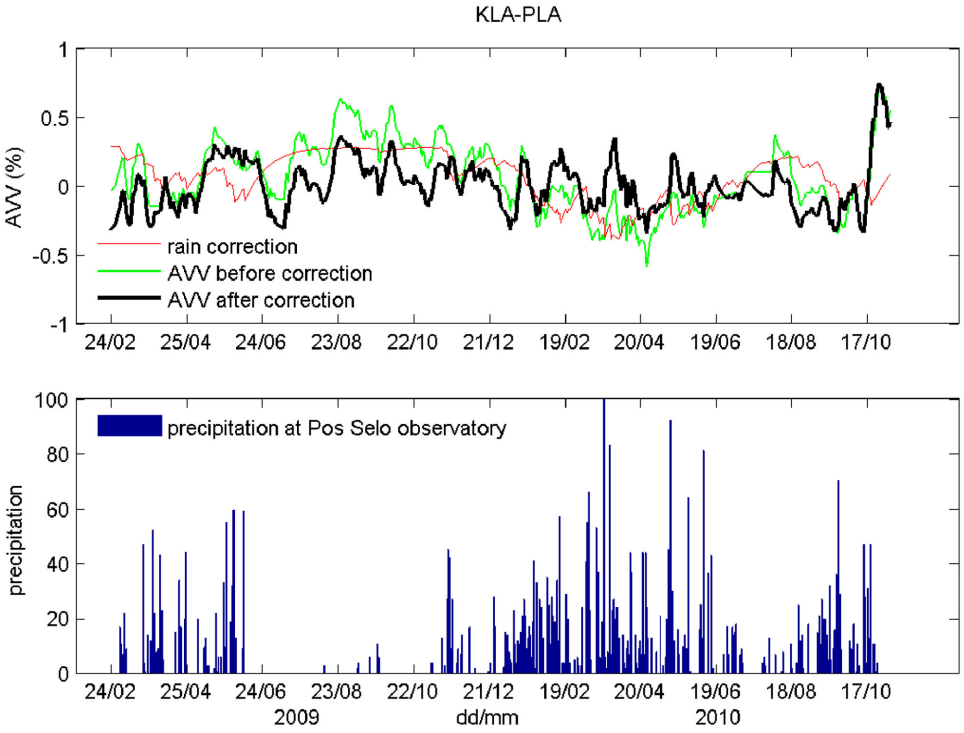

Figure 11. (a) Apparent velocity variations calculated for pair KLA-PLA in 2009 and 2010. Green line: raw AVV. Red line: velocity variations associated with rainfall calculated with a ground water level model. Black line: AVV corrected for rainfall effect. (b) Precipitation data (arbitrary unit) from Selo Observatory Post.

2008). Budi Santoso *et al*. (2013) suggested that it could correspond to a ductile layer of the Ancient Merapi left by the Holocene sector collapses (Newhall *et al*. 2000). The passing of the head of the magma intrusion through this aseismic layer was revealed by the upward migration of the hypocentres and by a temporary decrease of the seismicity level and the deformation rate (Surono *et al*. 2012).

Taking the available volcanological and geophysical observations into account, we propose a chronological interpretation of the observed phenomena in the framework of a magmatic intrusion. We divide the pre-eruptive period in six stages (Fig. 14). The beginning and end dates are indicative because they are not always well constrained and there are some overlaps between the stages. These stages correspond approximately to the six phases identified to describe the velocity variations (Section 4.4).

Stage 1: Feeding of magma storage zones (October 2009–September 2010)

Petrological studies suggest that there are several crystallization zones at different depths from 30 km to less than 10 km (Costa *et al*. 2013). Hotter and more volatile rich magma has probably feed the storage zones during the year preceding the eruption (Fig. 14a). This is indicated by the increase of the deformation rate from 0.3 to 1.2 mm d^{-1} and by the occurrence of several shallow seismic swarms, with some events belonging to multiplets 2, 3 and 6. These small bursts of seismic activity may have been triggered by heat and gas transfer from the deep magma body to the shallow layers and the hydrothermal system. No significant velocity changes were observed during this period although the calculated AVV display fluctuations that are mostly due to instrumental problems until beginning 2010.

Stage 2: Magma intrusion in deep conduit (September–mid October 2010)

A large batch of magma under strong over-pressure rose through the existing deep conduit. It produced damaging and fracturing of the surrounding rock and enlargement of the conduit (Fig. 14b). These processes are associated with the increase of the deep seismic activity at the beginning of September and with the acceleration of the deformation up to 8 cm d^{-1} (Surono *et al*. 2012). The shallow activity was also reactivated with the occurrence of more and more MP events, some VTB events per day and volcanic tremors observed mainly from 2010 September 20 to October 4. This reactivation may result from enhanced heat, steam and gas transfer from the ascending magma body and from stress changes in the shallow structure induced by the intrusion. Both deep and shallow multiplets were active during this stage. The rapid velocity decreases detected by CWI for deep multiplets 4 and 9 on 2010 October 11–12 are probably due to a velocity perturbation close to the corresponding hypocentres at about 2.7 km depth. However, no significant AVV is detected from NCF.

Stage 3: Magma migration through the aseismic zone (2010 October 12–20)

During this stage, a period of relative seismic quiescence took place. The rate of occurrence of VTB and MP events progressively increased, while the VTA activity was decreasing. Simultaneously, the deformation temporarily slowed down. A large velocity decrease, detected by all the shallow multiplets, started on 2010 October 13–14 and followed afterwards. The analysis of NCF showed marked velocity variations for most station pairs. These observations are

Downloaded from http://gji.oxfordjournals.org/ at Biblio Planets on May 20, 2016

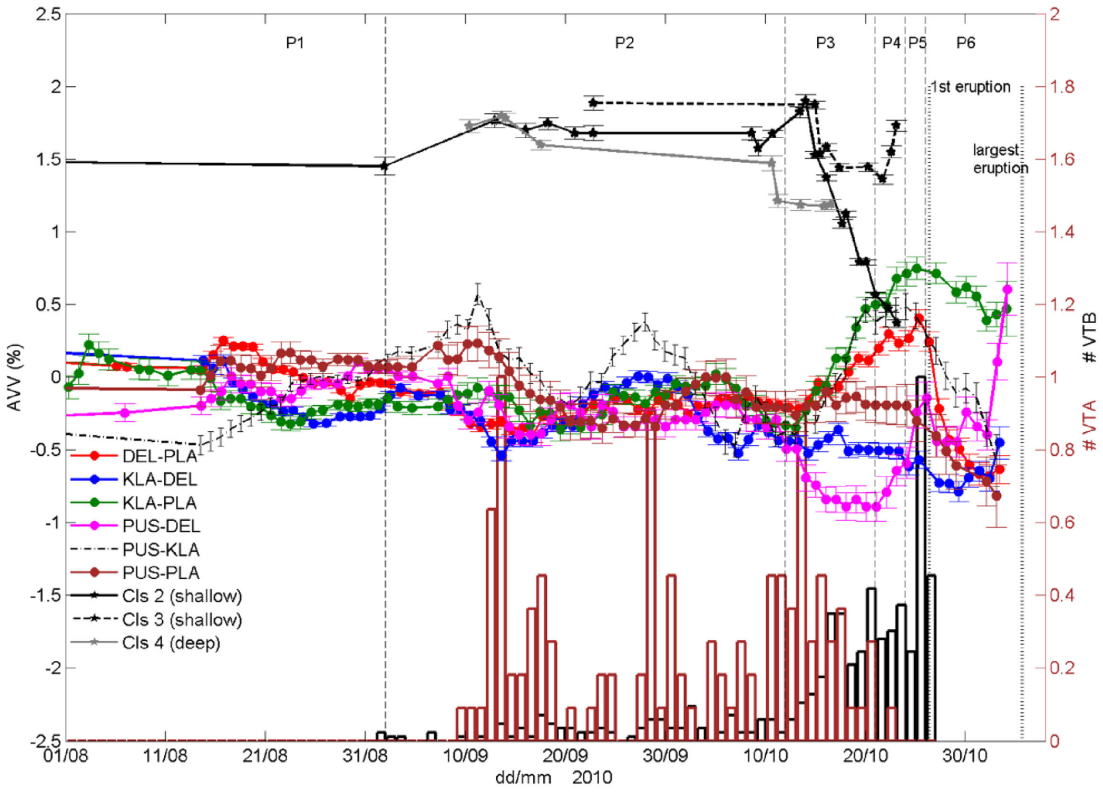

Figure 12. Synthetic view of the apparent velocity variations obtained from multiplets and NCF for the period of August–November 2010. Estimated errors are indicated by vertical bars. Vertical dashed lines indicate the boundaries of the phases (P1 to P6) used to describe the seismic activity and the AVV (see Section 4.3). Vertical dotted lines show eruptions of 26 October and 5 November. For clarity, only a selection of representative multiplets recorded at station PAS has been used here and the corresponding AVV have been shifted upward by +1.5 per cent. At the bottom, histograms of the daily numbers of VTA (brown) and VTB (black) events.

consistent with the progressive intrusion of magma through the ductile and aseismic zone between 1.5 and 2.5 km depth (Fig. 14c).

Stage 4: Intrusion in the shallow conduit (2010 October 20–24)

Once the head of the magma intrusion has reached the upper part of the plumbing system, it produced again rock damaging and enlargement of the conduit (Fig. 14d). The VTB seismic activity accelerated following a power law which allowed to apply in hindsight the material Failure Forecasting Method and to successfully estimate the date of the eruption onset (Budi-Santoso *et al*. 2013; Boué 2015; Boué *et al*. 2015). The stronger interaction between the degassing magma body and the shallow hydrothermal system produced fluid transfers which are probably involved in the generation of shallow VLP events and large LF earthquakes whose activity culminated on 2010 October 23–24 (Budi-Santoso *et al*. 2013; Jousset *et al*. 2013). The intrusion induced also the accelerated outward displacement of the southern part of the crater (Surono *et al*. 2012) and the increasing numbers of MP events and rockfalls. During this phase, the apparent velocity estimated for pair PUS–DEL turned to increase while the trends observed for the other pairs continued. The location of the perturbations shows patterns of velocity decrease in most of the upper flanks of the volcano (Fig. 13a).

Stage 5: Plug fracturing (2010 October 25–26)

During the last day before the eruption onset, the seismic activity increased sharply, with the occurrence of about 200 VTB and 600 MP events. The largest VTB events of the pre-eruptive sequence were recorded during this period. The deformation rate reached 50 cm d^{-1}, the highest level ever observed at Merapi. Thanks to the numerous events (~120 in 20 hr) belonging to multiplet 10, an estimation of the velocity variations could be obtained with an exceptionally high temporal resolution (Fig. 8). The velocity fluctuations revealed by the analysis of multiplet 10 suggests a process of progressive fracturation of the plug due to pulses of magma intrusion that produced material damaging (Fig. 14e). After each episodes of decreasing, that generally coincided with large VTB events, the velocity recovered its value, possibly due to rapid healing enhanced by fluid circulation. In particular, the largest VTB that occurred at 20:00 UT coincides with a sharp velocity decrease of about 0.4 per cent. This phenomenon may also result from the nonlinear elastic behaviour of the granular volcanic material and its mechanical softening produced by strong shaking (Lesage *et al*. 2014). During this stage, the pattern of velocity perturbations in the structure (Fig. 13b) was mostly similar to that of the preceding period (Fig. 13a), with a slight velocity increase in the northern flank.

Stage 6: Eruption onset (2010 October 26)

The last part of the plug eventually failed and the intrusion reached the surface on 2010 October 26, producing the initial explosive eruption at 10:02 UT (Fig. 14f). This event expelled about 6×10^6 m^3 of non-juvenile material, including the 2006 lava dome, and created a new crater (Pallister *et al*. 2013). It was followed by many

Downloaded from http://gji.oxfordjournals.org/ at Biblio Planets on May 20, 2016

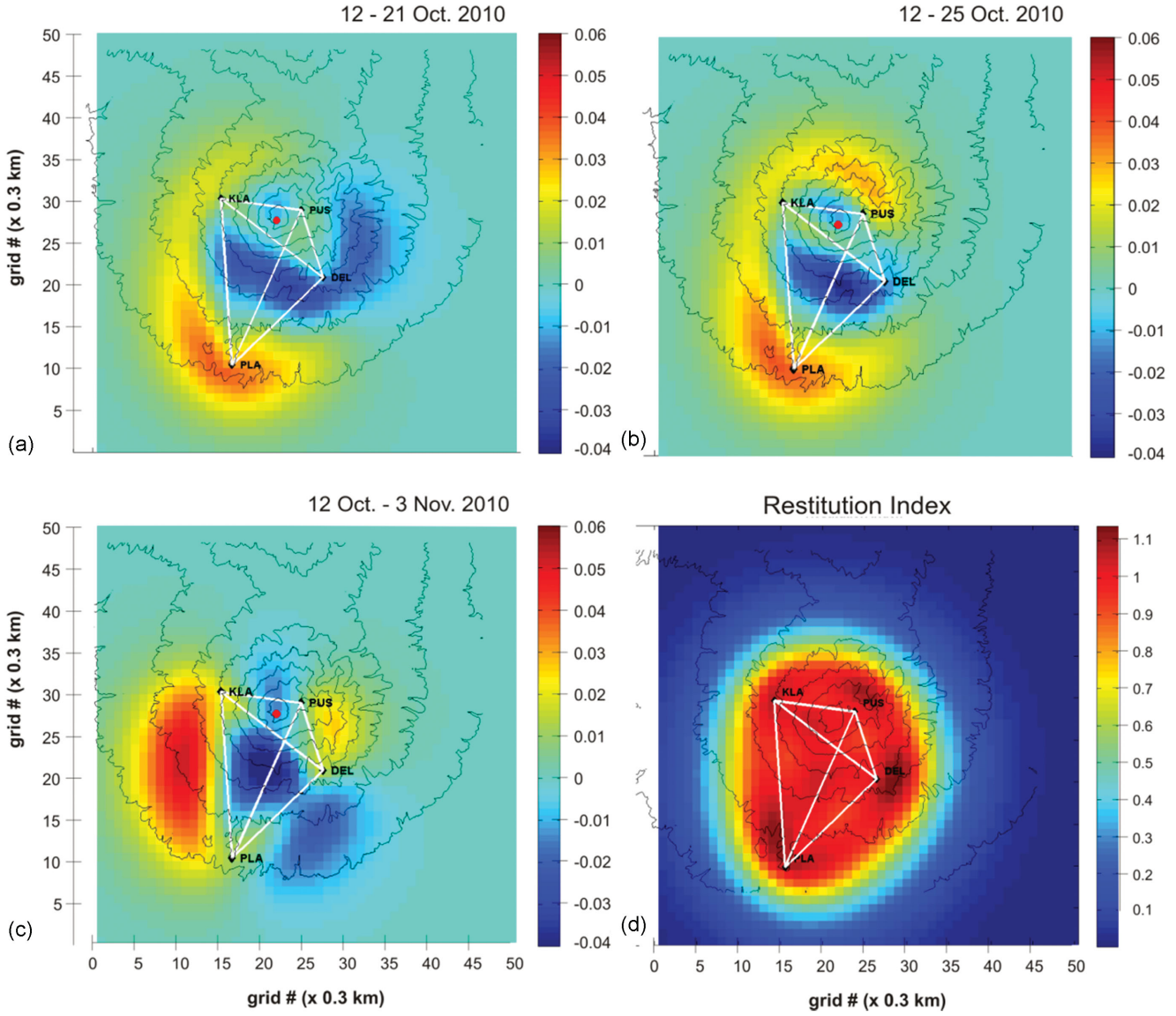

Figure 13. Location of the velocity perturbations estimated for three periods that end on 21 October, 25 October and 3 November (panels a–c, respectively). All the periods begin on 12 October. The four permanent stations are indicated by black diamonds and the six station pairs by white lines. The position of the summit is shown by a red circle. (d) Map of corresponding restitution index. Velocity perturbations can be recovered only in regions where the restitution index is close to one.

additional explosions and a phase of very large discharge rate producing a new lava dome, which indicates that the magmatic system was totally open. After the eruption onset, the apparent velocity decreased for all the station pairs and the pattern of velocity change distribution was strongly modified (Fig. 13c). The opening of the system and the destruction of the old dome probably induced pressure decrease in the conduit, stress release in the surrounding structure, and velocity decrease in the non-damaged part of the structure.

6 CONCLUSIONS

The observations provided by the permanent monitoring system of Merapi volcano and some temporary stations were of paramount importance in evaluating the level of risk during the 2010 crisis and for supporting timely and appropriate decisions of evacuation. It is also important to carry out a posteriori in depth re-analysis of the data as it helps understanding the volcanic processes involved in the preceding eruption and it may help interpreting the precursors of future eruptive crises as well as improving monitoring methods. In spite of some instrumental limitations, the data set obtained provided the opportunity of estimating velocity variations in a period of about 1 yr that includes the 2010 explosive sequence. For the first time to our knowledge, the technique of CWI could be applied to both correlation functions of seismic noise and to several series of events with similar waveforms. The results display a complex pattern of variations with simultaneous increases and decreases of velocity according to the station pair used and non-synchronised changes obtained from multiplets. Most of these variations occurred in the last 2 weeks before and just after the eruption onset.

The location of the velocity perturbations in the structure, estimated using an approach based on diffuse wavefields, shows also complex spatial distribution which varies with time. Before the eruption onset, velocity decreases occurred mainly in the upper

Downloaded from http://gji.oxfordjournals.org/ at Biblio Planets on May 20, 2016

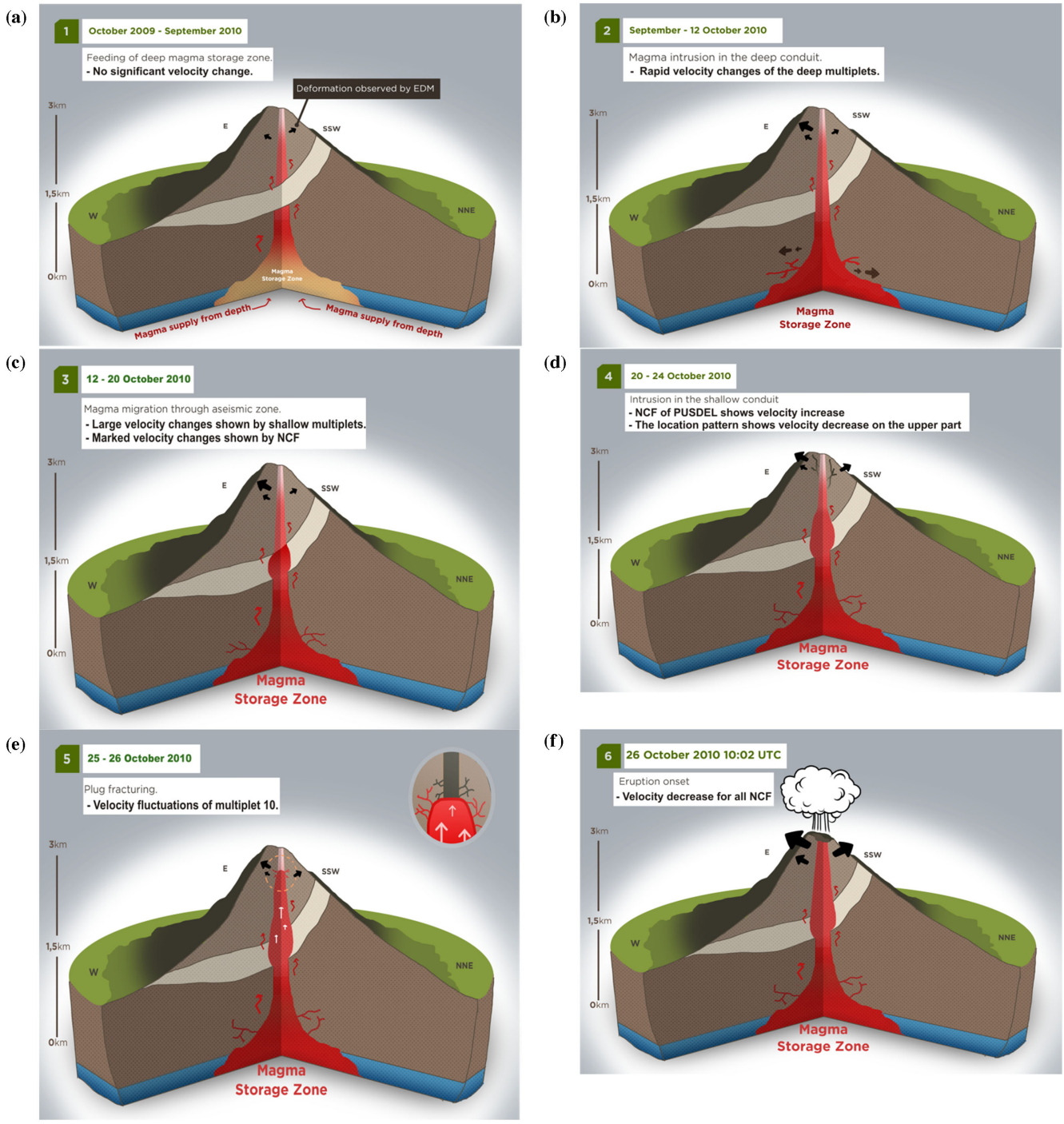

Figure 14. Interpretative model of the magmatic intrusion and the seismic activities prior to the eruption of 2010 October 26. The simplified geological structure is adopted from Camus *et al*. (2000) and Müller & Haak (2004). The yellow area represents the ductile and aseismic layer of the Ancient Merapi. The location and size of the structures are not precise.

southern flank of the volcano and close to the crater, while velocity seems to have increased in the lower parts of the edifice. The distribution was strongly modified after the explosive eruption of 2010 October 26 and the opening of the magmatic system. The complicated pattern of spatial and temporal velocity variations can be interpreted as the effect of stress changes in the structure due to the propagation of a large magmatic intrusion. The seismic velocities of volcanic rocks are much more sensitive to stress variations than other types of rock because they are strongly microfractured and porous. When stresses rise, velocities strongly increase. Moreover, over a given threshold of deviatoric stress, new cracks appear and propagate, producing rock damage and large velocity decrease. Thus depending on the position of the intrusion and the distribution of the associated stress field, increases and decreases of the rock velocities can occurred simultaneously in different parts of the structure. The resulting AVVs estimated by CWI can have

Downloaded from http://gji.oxfordjournals.org/ at Biblio Planets on May 20, 2016

positive or negative sign according to the position of the stations used.

The main features of the 2010 pre-eruptive seismic activity suggest that a large volume of magma rapidly intruded the structure in the few weeks before the eruption. This is consistent with the large anelastic deformation of the crater, the high level of seismic energy release and seismicity rate, the migration of the sources of VT events, and the observed velocity variations. The large batch of intruding magma probably produced enlargement of the conduit and damaging of the surrounding rocks, which can explain why the materiel failure forecasting method (Voight 1988) gave encouraging results for the forecast of the eruption onset using VT seismicity (Budi-Santoso *et al*. 2013; Boué 2015; Boué *et al*. 2015). This damaging produced rock permeability increase close to the conduit and stimulated heat and fluid transfers yielding strong low-frequency seismicity.

Although the detailed interpretation and modelling of the velocity variations are still quite challenging, due to the complexity of observations and of the relationship between them and stress variations, we proposed a scenario of the magma intrusion in six stages that integrates all the geophysical data. According to our interpretative framework, the detected AVVs can be considered as precursors of volcanic eruptions in andesitic volcanoes, without taking their sign into account. This kind of precursor could be used and studied more in detail before future eruptions by using broadband seismometers and by improving the density of seismic stations on and around the volcano.

ACKNOWLEDGEMENTS

We acknowledge the staff of BPPTKG and CVGHM for their support in keeping the network working. We thank the Ministry of Energy and Mineral Resources of Indonesia for a doctoral scholarship granted to ABS. This work was partially supported by ANR-12-BS06-0012-01 DOMERAPI project of the Agence Nationale de la Recherche, the Coopération Franco-Indonésienne funded by the French Ministère des Affaires Etrangères, the Université Savoie Mont Blanc, and by the Institut de Recherche pour le Développement. We appreciated discussions and suggestions from Eric Larose, Jean-Luc Got and Michael Heap. We thank two anonymous reviewers whose comments greatly improved the manuscript.

REFERENCES

Anggono, T., Nishimura, T., Sato, H., Ueda, H. & Ukawa, M., 2012. Spatio-temporal changes in velocity associated with 2000 activity of Miyakejima volcano as inferred from cross-correlation analyses of ambient noise, *J. Volc. Geotherm. Res.,* **247–248,** 93–107.

Battaglia, J., Métaxian, J.-P. & Garaebiti, E., 2012. Earthquake-volcano interaction imaged by coda wave interferometry, *Geophys. Res. Lett.,* **39,** L11309, doi:10.1029/2012GL052003.

Bensen, G.D., Ritzwoller, M.H., Barmin, M.P., Levshin, A.L., Lin, F., Moschetti, M.P., Shapiro, N.M. & Yang, Y., 2007. Processing seismic ambient noise data to obtain reliable broad-band surface wave dispersion measurements, *Geophys. J. Int.,* **169,** 1239–1260.

Birch, F., 1960. The velocity of compressional waves in rocks to 10 kilobars, *J. geophys. Res.* **65,** 1083, doi:10.1029/JZ065i004p01083.

Boué, A., 2015. Data mining and volcanic eruption forecasting, *PhD thesis,* University of Grenoble, Grenoble, France.

Boué, A., Lesage, P., Cortés, G., Valette, B. & Reyes-Dávila, G., 2015. Real-time eruption forecasting using the material Failure Forecast Method with a Bayesian approach. *J. geophys. Res.,* **120**(4), 2143–2161.

Brenguier, F., Campillo, M., Takeda, T., Aoki, Y., Shapiro, N.M., Briand, X., Emoto, K. & Miyake, H., 2014. Mapping pressurized volcanic fluids from induced crustal seismic velocity drops, *Science,* **345,** 80–82.

Brenguier, F., Shapiro, N.M., Campillo, M., Ferrazzini, V., Duputel, Z., Coutant, O. & Nercessian, A., 2008. Towards forecasting volcanic eruptions using seismic noise, *Nat. Geosci.,* **1,** 126–130.

Budi-Santoso, A., 2014. The seismic activity associated with the large 2010 eruption of Merapi volcano, Java: source location, velocity variation, and forecasting, *PhD thesis,* University of Grenoble, Grenoble, France.

Budi-Santoso, A., Lesage, P., Dwiyono, S., Sumarti, S., Subandriyo, Surono, Jousset, P. & Metaxian, J.-P., 2013. Analysis of the seismic activity associated with the 2010 eruption of Merapi Volcano, Java, *J. Volc. Geotherm. Res.,* **261,** 153–170.

Campillo, M. & Paul, A., 2003. Long-range correlations in the diffuse seismic coda, *Science,* **299,** 547–549.

Camus, G., Gourgaud, A., Mossand-Berthommier, P.C. & Vincent, P.M., 2000. Merapi (Central Java, Indonesia): an outline of the structural and magmatological evolution, with a special emphasis to the major pyroclastic events, *J. Volc. Geotherm. Res.,* **100,** 139–163.

Cannata, A., 2012. Crustal changes at Mt. Etna volcano accompanying the 2002–2003 eruption as inferred from a repeating earthquake analysis. *Geophys. Res. Lett.,* **39,** L18311, doi:10.1029/2012GL053185.

Clarke, D., Zaccarelli, L., Shapiro, N.M. & Brenguier, F., 2011. Assessment of resolution and accuracy of the Moving Window Cross Spectral technique for monitoring crustal temporal variations using ambient seismic noise, *Geophys. J. Int.,* **186,** 867–882.

Costa, F., Andreastuti, S., Bouvet de Maisonneuve, C. & Pallister, J., 2013. Petrological insights into the storage conditions, and magmatic processes that yielded the centennial 2010 Merapi explosive eruption, *J. Volc. Geotherm. Res.,* **261,** 209–235.

Eberhart-Phillips, D., Han, D-H. & Zoback, M.D., 1989. Empirical relationships among seismic velocity, effective pressure, porosity, and clay content in sandstone, *Geophysics,* **54**(1), 82–89.

Froment, B., 2011. Utilisation du bruit sismique ambiant dans le suivi temporel de structures géologiques, *PhD thesis,* Université de Grenoble, Grenoble, France.

Froment, B., Campillo, M., Roux, P., Gouédard, P., Verdel, A. & Weaver, R., 2010. Estimation of the effect of non-isotropic distributed energy on the apparent arrival time in correlations, *Geophysics,* **75**(5), SA85–SA93.

Got, J.L. & Coutant, O., 1997. Anisotropic scattering and travel time delay analysis in Kilauea volcano, Hawaii, earthquake coda waves, *J. geophys. Res.,* **102,** 8397–8410.

Got, J.L., Peltier, A., Staudacher, T., Kowalski, P. & Boissier, P., 2013. Edifice strength and magma transfer modulation at Piton de la Fournaise volcano, *J. geophys. Res.,* **118,** 5040–5057.

Han, L., Wong, J., Bancroft, C.J. & Stewart, R.R., 2008. Automatic time picking and velocity determination on full waveform sonic well logs, in CREWES Research Report Volume 20.

Hansen, B.E., 1992. Testing for parameter instability in linear models, *J. Policy Model.,* **14,** 517–533.

Heap, M.J., Baud, P., Meredith, P.G., Vinciguerra, S. & Reuschlé, T., 2014a. The permeability and elastic moduli of tuff from Campi Flegrei, Italy: implications for ground deformation modelling, *Solid Earth,* **5**(1), 25–44.

Heap, M.J., Lavallée, Y., Petrakova, L., Baud, P., Reuschlé, T., Varley, N.R. & Dingwell, D.B., 2014b. Microstructural controls on the physical and mechanical properties of edifice-forming andesites at Volcán de Colima, Mexico, *J. geophys. Res.,* **119**(4), 2925–2963.

Hidayati, S., Ishihara, K., Iguchi, M. & Ratdomopurbo, A., 2008. Focal mechanism of volcano-tectonic earthquakes at Merapi volcano, Indonesia, *Indonesian J. Phys.,* **19**(3), 75–82.

Jousset, P., Budi-Santoso, A., Jolly, A.D., Boichu, M., Surono, Dwiyono, S., Sumarti, S., Hidayati, S. & Thierry, P., 2013. Signs of magma ascent in LP and VLP seismic events and link to degassing: an example from the 2010 explosive eruption at Merapi volcano, Indonesia, *J. Volc. Geotherm. Res.,* **261,** 171–192.

Downloaded from http://gji.oxfordjournals.org/ at Biblio Planets on May 20, 2016

Koulakov, I. *et al.*, 2007. *P* and *S* velocity structure of the crust and the upper mantle beneath central Java from local tomography inversion, *J. geophys. Res.,* **112**(B8), B08310, doi:10.1029/2006JB004712.

Larose, E., Derode, A., Campillo, M. & Fink, M., 2004. Imaging from one-bit correlations of wideband diffuse wave fields, *J. Appl. Phys.,* **95**(12), 8393–8399.

Larose, E., Planes, T., Rossetto, V. & Margerin, L., 2010. Locating a small change in a multiple scattering environment, *Appl. Phys. Lett.,* **96**(20), 204101, doi:http://dx.doi.org/10.1063/1.3431269.

Lesage, P., Arámbula-Mendoza, R. & Reyes-Dávila, G., 2014. Large tectonic earthquakes induce sharp temporary decreases in seismic velocity in Volcán de Colima, Mexico, *J. geophys. Res.,* **119,** 4360–4376.

Lobkis, O.I. & Weaver, R.L., 2003. Coda-wave interferometry in finite solids: recovery of *P*-to-*S* conversion rates in an elastodynamic billiard, *Phys. Rev. Lett.,* **90**(25), doi:10.1103/PhysRevLett.90.254302.

Lockner, D.A., Walsh, J.B. & Byerlee, J.D., 1977. Changes in seismic velocity and attenuation during deformation of granite, *J. geophys. Res.,* **82**(33), 5374–5378.

Mavko, G., Mukerji, T. & Godfrey, N., 1995. Predicting stress-induced velocity anisotropy in rocks, *Geophysics* **60**(4), 1081–1087.

Mordret, A., Jolly, A.D., Duputel, Z. & Fournier, N., 2010. Monitoring of phreatic eruptions using Interferometry on retrieved cross-correlation function from ambient seismic noise: results from Mt. Ruapehu, New Zealand, *J. Volc. Geotherm. Res.,* **191**(1–2), 46–59.

Müller, A. & Haak, V., 2004. 3-D modeling of the deep electrical conductivity of Merapi volcano (Central Java): integrating magnetotellurics, induction vectors and the effects of steep topography, *J. Volc. Geotherm. Res.,* **138,** 205–222.

Nagaoka, Y., Nishida, K., Aoki, Y. & Takeao, M., 2010. Temporal change of phase velocity beneath Mt. Asama, Japan, inferred from coda wave interferometry, *Geophys. Res. Lett.,* **37,** L22311, doi:10.1029/2010GL045289.

Newhall, C.G. *et al.*, 2000. 10,000 Years of explosive eruptions of Merapi Volcano, Central Java: archaeological and modern implications, *J. Volc. Geotherm. Res.,* **100,** 9–50.

Nishimura, T. *et al.*, 2005. Temporal changes in seismic velocity of the crust around Iwate volcano, Japan, as inferred from analyses of repeated active seismic experiment data from 1998 to 2003, *Earth Planets Space,* **57**(6), 491–505.

Nishimura, T., Uchida, N., Sato, H., Ohtake, M., Tanaka, S. & Hamaguchi, H., 2000. Temporal changes of the crustal structure associated with the M6.1 earthquake on September 3, 1998, and the volcanic activity of Mount Iwate, Japan, *Geophys. Res. Lett.,* **27**(2), 269–272.

Nur, A., 1971. Effects of stress on velocity anisotropy in rocks with cracks, *J. geophys. Res.,* **76**(8), 2022–2034.

Obermann, A., Planès, T., Larose, E. & Campillo, M., 2013. Imaging preeruptive and coeruptive structural and mechanical changes of a volcano with ambient seismic noise, *J. geophys. Res.: Solid Earth,* **118,** 6285–6294.

Paasschens, J.C.J., 1997. Solution of the time-dependent Boltzmann equation, *Phys. Rev. E,* **56,** 1135–1141.

Pacheco, C. & Snieder, R., 2005. Time-lapse travel time change of multiply scattered acoustic waves, *J. acoust. Soc. Am.,* **118,** 1300–1310.

Pallister, J.S., Schneider, D.J., Griswold, J.P., Keeler, R.H., Burton, W.C., Noyles, C., Newhall, C.G. & Ratdomopurbo, A., 2013. Merapi 2010 eruption—Chronology and extrusion rates monitored with satellite radar and used in eruption forecasting, *J. Volc. Geotherm. Res.,* **261,** 144–152.

Planès, T., 2013. Imagerie de changements locaux en régime de diffusion multiple, *PhD thesis,* Université de Grenoble, Grenoble, France.

Poupinet, G., Ellsworth, W.L. & Fréchet, J., 1984. Monitoring velocity variations in the crust using earthquake doublets: an application to the Calaveras fault, California, *J. geophys. Res.,* **89,** 5719–5731.

Ratdomopurbo, A. & Poupinet, G., 2000. An overview of the seismicity of Merapi volcano (Java, Indonesia), 1983–1994, *J. Volc. Geotherm. Res.,* **100,** 193–214.

Ratdomopurbo, A., 1995. Etude Sismologique du Volcan Merapi et Formation du dôme de 1994, *PhD thesis,* Université Joseph Fourier-Grenoble I, France.

Ratdomopurbo, A. & Poupinet, G., 1995. Monitoring a temporal change of seismic velocity in a volcano: application to the 1992 eruption of Mt. Merapi (Indonesia), *Geophys. Res. Lett.,* **22**(7), 775–778.

Rivet, D., Brenguier, F., Clarke, D., Shapiro, N.M. & Peltier, A., 2014. Long-term dynamics of Piton de la Fournaise volcano from 13 years of seismic velocity change measurements and GPS observations, *J. geophys. Res.,* **119**, doi:10.1002/2014JB011307.

Rocchi, V., Sammonds, P.R. & Kilburn, C.R.J., 2004. Fracturing of Etnean and Vesuvian rocks at high temperatures and low pressures, *J. Volc. Geotherm. Res*., **132,** 137–157.

Rubinstein, J.L., Uchida, N. & Beroza, G.C., 2007. Seismic velocity reductions caused by the 2003 Tokachi-Oki earthquake, *J. geophys. Res.,* **112,** B05315, doi:10.1029/2006JB004440.

Sabra, K.G., Gerstoft, P., Roux, P., Kuperman, W.A. & Fehler, M., 2005. Extracting time-domain Green's function estimates from ambient seismic noise, *Geophys. Res. Lett.,* **32,** L03310, doi:10.1029/2004GL021862.

Saragiotis, C.D., Hadjileontiadis, L.J. & Panas, S.M., 2002. PAI-S/K: a robust automatic seismic P phase arrival identification scheme, *IEEE Trans. Geosci. Remote Sens.,* **40,** 1395–1404.

Sato, H., 1993. Energy transportation in one- and two-dimensional scattering media: analytic solutions of the multiple isotropic scattering model, *Geophys. J. Int.,* **112,** 141–146.

Sens-Schönfelder, C., 2008. Synchronizing seismic networks with ambient noise, *Geophys. J. Int.,* **174,** 966–970.

Sens-Schönfelder, C. & Wegler, U., 2006. Passive image interferometry and seasonal variations of seismic velocities at Merapi Volcano, Indonesia, *Geophys. Res. Lett.,* **33,** L21302, doi:10.1029/2006GL027797.

Sens-Schönfelder, C., Pomponi, E. & Peltier, A., 2014. Dynamics of Piton de la Fournaise volcano observed by passive image interferometry with multiple references, *J. Volc. Geotherm. Res.,* **276,** 32–45.

Shang, T. & Gao, L., 1988. Transportation theory of multiple scattering and its application to seismic coda waves of impulsive source, *Sci. Sin.,* **31,** 1503–1514.

Shapiro, S.A., 2003. Elastic piezosensitivity of porous and fractured rocks, *Geophysics,* **68,** 482–486.

Snieder, R., 2006. The theory of coda wave interferometry, *Pure appl. Geophys.,* **163**(2), 455–473.

Stanchits, S., Vinciguerra, S. & Dresen, G, 2006. Ultrasonic velocities, acoustic emission characteristics and crack damage of basalt and granite, *Pure appl. Geophys*., **163,** 974–993.

Stehly, L., Campillo, M. & Shapiro, N.M., 2007. Traveltime measurements from noise correlation: stability and detection of instrumental time-shifts, *Geophys. J. Int.,* **171,** 223–230.

Surono *et al.*, 2012. The 2010 explosive eruption of Java's Merapi volcano—a '100-year' event, *J. Volc. Geotherm. Res.,* **241–242,** 121–135.

Tarantola, A. & Valette, B., 1982. Generalized nonlinear inverse problems solved using the least squares criterion, *Rev. Geophys.,* **20,** 219–232.

Vergely, J.L., Valette, B., Lallement, R. & Raimond, S., 2010. Spatial distribution of interstellar dust in the Sun's vicinity—comparison with neutral sodium-bearing gas, *Astron. Astrophys.,* **518,** A31, doi:10.1051/0004-6361/200913962.

Voight, B., 1988. A method for prediction of volcanic eruptions, *Nature,* **332,** 125–130.

Voight, B., Sukhyar, R. & Wirakusumah, A.D., 2000. Introduction to the special issue on Merapi volcano, *J. Volc. Geotherm. Res.,* **100,** 1–8.

Waldhauser, F. & Ellsworth, W.L., 2000. A double-difference earthquake location algorithm: method and application to the Northern Hayward Fault, California, *Bull. seism. Soc. Am.,* **90,** 1353–1368.

Wassermann, J. & Ohrnberger, M., 2001. Automatic hypocenter determination of volcano induced seismic transients based on wavefield coherence—an application to the 1998 eruption of Mt. Merapi, Indonesia, *J. Volc. Geotherm. Res.,* **110,** 57–77.

Weaver, R. & Lobkis, O.I., 2001. Ultrasonics without a source: thermal fluctuation correlations at MHz frequencies, *Phys. Rev. Lett.,* **87**(13), 134301, doi:http://dx.doi.org/10.1103/PhysRevLett.87.134301.

Downloaded from http://gji.oxfordjournals.org/ at Biblio Planets on May 20, 2016

Weaver, R., Froment, B. & Campillo, M., 2009. On the correlation of non-isotropically distributed ballistic scalar diffuse waves, *J. acoust. Soc. Am.,* **126,** 1817–1826.

Wegler, U. & Lühr, B.-G., 2001. Scattering behavior at Merapi volcano (Java) revealed from an active seismic experiment, *Geophys. J. Int.,* **145**(3), 579–592.

Wegler, U., Lühr, B.-G., Snieder, R. & Ratdomopurbo, A., 2006. Increase of shear wave velocity before the 1998 eruption of Merapi volcano (Indonesia), *Geophys. Res. Lett.,* **33,** L09303, doi:10.1029/2006GL025928.

West, M., 2008. Tools and topics in seismic waveform cross-correlation, Available at: http://www.giseis.alaska.edu/Seis/EQ/tools/GISMO/#CORRELATION, last accessed 15 August 2013.

Zimmerman, R.W., Somerton, W.H. & King, M.S., 1986. Compressibility of porous rocks, *J. geophys. Res.,* **91**(B12), 12 765–12 777.

Zulfakriza, Z., Saygin, E., Cummins, P.R., Widiyantoro, S., Nugraha, A.D., Lühr, B.-G. & Bodin, T., 2014. Upper crustal structure of central Java, Indonesia, from transdimensional seismic ambient noise tomography, *Geophys. J. Int.,* **197,** 630–635.

APPENDIX A: METHOD OF FIRST ARRIVAL PICKING BY THE LONG-TERM TO SHORT-TERM ENERGY RATIO (*LTE/STE*)

We propose here a method to improve the classical *STA/LTA* algorithm used for event detection and arrival time picking. This improvement was required by the poor precision of *STA/LTA* in picking the first arrival of some kinds of event, such as emergent signals. In our approach, the events are first detected by the *STA/LTA* procedure which provides a rough estimation of the arrival times. In a second step, we calculate the ratio between the long-term and the short-term energy averages (*LTE/STE*) which gives more precise estimations of the arrival times.

The short-term energy average *STE* and the long-term energy average *LTE* are defined as:

$$STE_i = \frac{1}{ns} \sum_{j=i-ns}^{i} x_j^2$$

$$LTE_i = \frac{1}{nl} \sum_{j=i-nl/2}^{i+nl/2} x_j^2,$$

where *ns* and *nl* are the lengths, in samples, of the short and long windows, respectively, x_j are signal samples, and *i* corresponds to the current time. Note that sample *i* is at the end of the short window while it is at the middle of the long one. Thus the long window is the first to include the onset of an event, producing the increase of LTE and LTE/STE. When the short term window (STE) reaches the onset, the ratio of LTE/STE sharply decreases (Fig. A1). The arrival time is given by the position of the maximum of the absolute value of the derivative of LTE/STE in a small (5 s) window around the time estimated by STA/LTA. In the present study, we used $ns = 100$ samples (1 s) and $nl = 300$ samples (3 s).

We carried out several tests with synthetic and real seismograms in order to compare the results obtained with the LTE/STE ratio with those given by manual picking, STA/LTA algorithm, and methods based on the use of kurtosis (Saragiotis *et al*. 2002) and Modified Energy Ratio (Han *et al*. 2008). We found that the LTE/STE method provides relatively stable results, even in the presence of noise, with very small standard deviations with respect to the manually picked arrival times (Budi-Santoso 2014).

APPENDIX B: INFLUENCE OF THE AMPLITUDE NORMALIZATION

The one bit normalization commonly used to reduce the influence of seismic events in the calculation of noise correlation functions (Larose *et al*. 2004; Bensen *et al*. 2007) is equivalent to a strong

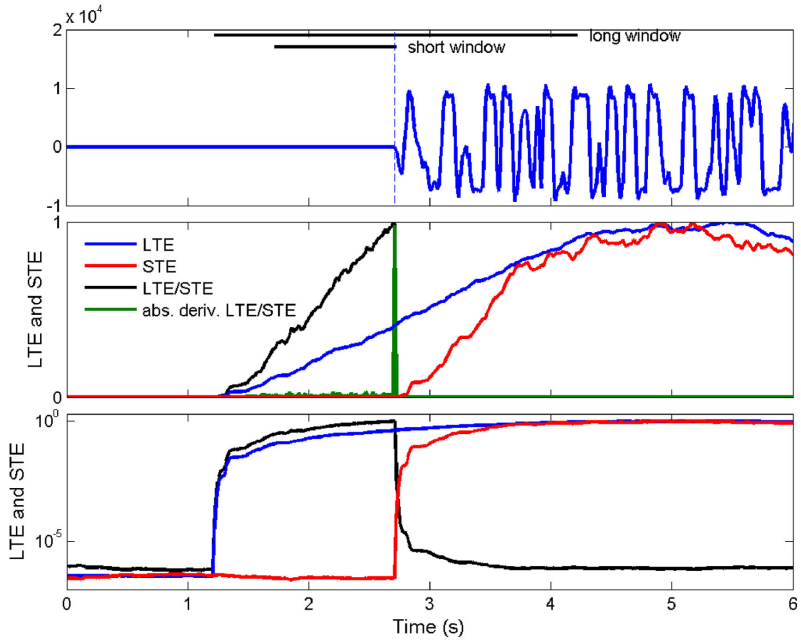

Figure A1. Illustration of the LTE/STE method. Top panel: seismogram with manually picked arrival time (vertical dashed line); middle panel: STE, LTE, LTE/STE and absolute value of derivative with linear scales; bottom panel: same with logarithmic scales. The current time is at the middle of the LTE window and at the end of the STE window. These windows are displayed as horizontal bars in top panel. The arrival time is set when the ratio LTE/STE decreases dramatically, which corresponds to the maximum of the absolute value of the derivative of LTE/STE.

Downloaded from http://gji.oxfordjournals.org/ at Biblio Planets on May 20, 2016

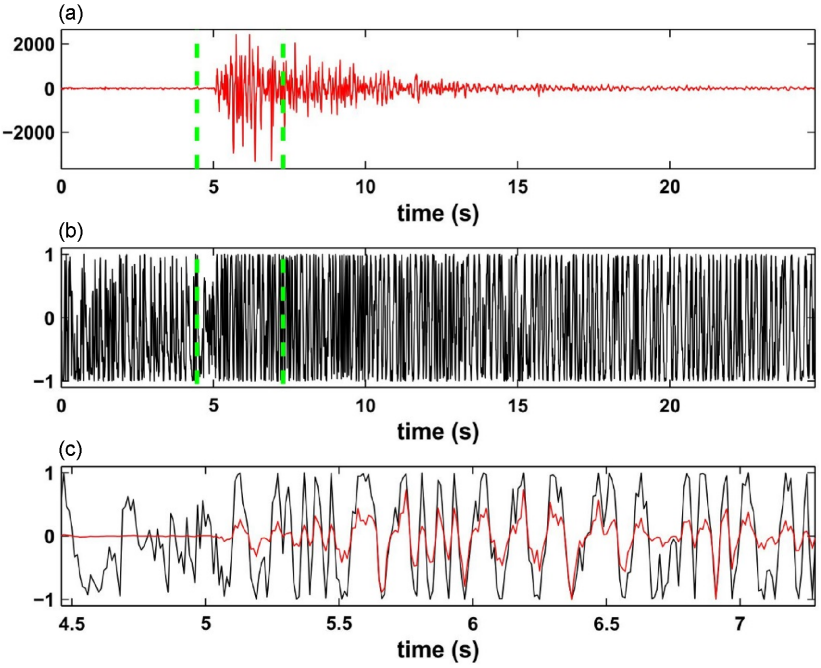

Figure B1. Example of amplitude normalization by the signal envelope. (a) Seismic event recorded at station PUS; (b) normalized signal; (c) enlargement of the sections between vertical green lines in (a) and (b).

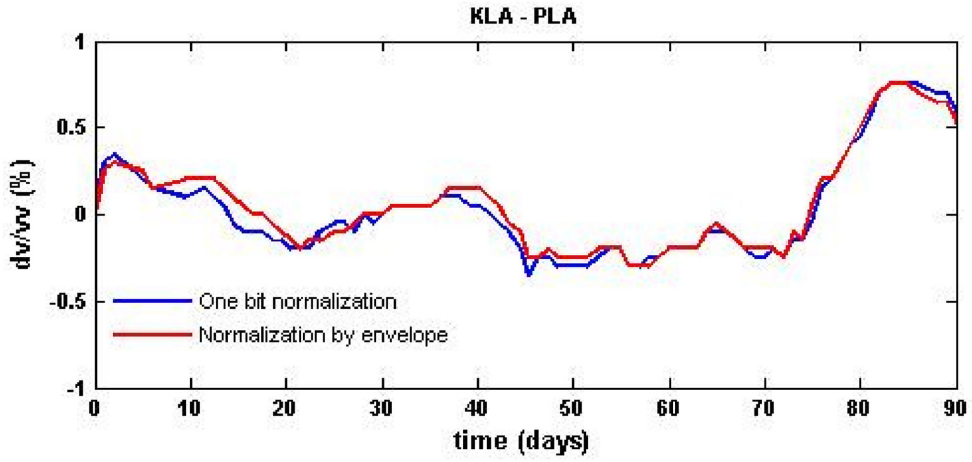

Figure B2. Comparison of time-series of apparent velocity variations for pair KLA-PLA from August to October 2010. The corresponding NCF have been calculated using either one bit normalization (blue) or normalization by the signal envelope (red). The frequency bandwidth used in these calculations is [0.125–2] Hz.

clipping of the signal. For example, this process transforms a sine into a rectangular function of the same frequency f_0. The spectrum of the latter function contains harmonics peaks at frequencies $3f_0$, $5f_0 \ldots$ with amplitudes decreasing as the inverse of frequency. Thus, the one bit normalization generates high frequency noise that might modify the real components of the wavefield and produce spurious features in the NCF (Sabra *et al*. 2005).

In order to evaluate the importance of this effect, we compare NCF calculated using the one bit normalization with NCF obtained with another approach. We introduce here a new normalization which consists in dividing the signal $x(t)$ by its envelope $e(t)$:

$$x_{\mathrm{norm}}(t) = \frac{x(t)}{\mathrm{e}(t)} \text{ with } \mathrm{e}(t) = \sqrt{x^2(t) + \tilde{x}^2(t)},$$

where $\tilde{x}(t) = TH[x(t)]$ is the Hilbert Transform of the signal. This type of amplitude normalization does not produce any clipping of the signal, but it is more computer time consuming. Fig. B1 displays a record that contains noise and a seismic event, the corresponding normalized signal, and an enlargement of both signals. It shows that the amplitude of the normalized signal, before and after the arrival of the event, is approximately constant and that it is in phase with the original signal. The NCF calculated with the two types of normalization are almost identical and the corresponding AVVs are very similar (Fig. B2). We conclude that the one bit normalization does not produce major artefacts and that it can be used even with relatively large bandwidth seismic noise.

Downloaded from http://gji.oxfordjournals.org/ at Biblio Planets on May 20, 2016